Chapter 8

CYCLIC FATIGUE

Fatigue is the phenomenon of mechanical property degradation under cyclic loading. The cyclic loads may be mechanical, thermal, or a combination of the two. Many high-volume applications of composite materials involve cyclic-loading situations, e.g., automobile components, aircraft structures, etc. Below we provide a brief description of the two main approaches that have been used to quantify fatigue behavior of materials (for a more complete description, the reader may consult the texts by Meyers and Chawla (1999) and Suresh (1998).

Stress versus cycles (S-N): This approach involves cyclic fatigue testing to develop *S-N* curves, where S is the stress amplitude and *N* is the number of cycles to failure. In general, for ferrous metals, a clear fatigue limit or endurance limit is observed. For stress levels below this endurance limit, theoretically, the material can be cycled infinitely without failure. In nonferrous materials, such as aluminum, a true endurance limit does not exist. Here one can arbitrarily define a certain number of cycles, say 10^7, as a point of "fatigue runout," at which point the experiment is stopped. The fatigue behavior of structural materials can be conveniently divided into two stages: crack initiation and propagation. In high cycle fatigue (HCF) of metals, most of the fatigue life is spent initiating a fatigue crack and a very small fraction of the life is spent in propagation. In low cycle fatigue (LCF), a much larger fraction of the fatigue life is spent in crack propagation. The phenomena of work hardening and work softening also play a more important role in LCF. One major drawback of the *S-N* approach is that no distinction can be made between the crack initiation phase and the crack propagation phase.

Fatigue crack growth: This approach is based on fracture mechanics and it enables the study of fatigue crack propagation. Fatigue crack propagation experiments are generally conducted on notched samples. The crack length,

a, is measured as a function of fatigue cycles, N, over a range of cyclic stress intensity factors, ΔK. The applied cyclic stress intensity range is given by:

$$\Delta K = Y\Delta\sigma\sqrt{\pi a}$$

where Y is a geometric parameter that depends on the nature of the notch and specimen configuration, $\Delta\sigma$ is the cyclic stress range, and a is the crack length. The results are then presented as log da/dN (crack growth per cycle) versus log ΔK. Crack growth rate, da/dN, is related to ΔK according to the power-law relationship first formulated by Paris et al. (1961, 1963):

$$\frac{da}{dN} = C(\Delta K)^m$$

where C and m are constants that depend on the material and test conditions.

The application of a fracture mechanics based approach to composites is not straightforward. The main reason for this is the inherent heterogeneity and anisotropic nature of the composites. These attributes of composites result in damage mechanisms that are very different from those encountered in conventional, homogeneous materials. Despite these limitations, conventional approaches have been used and modified to quantify the fatigue behavior of composites. As in previous chapters, we divide our discussion of fatigue into two major types of MMCs: continuous fiber reinforced and discontinuously reinforced (primarily particle reinforced) MMCs.

8.1 STRESS VERSUS CYCLES (S-N) FATIGUE

Several material variables play an important role in fatigue of MMCs. These include modulus, strength, ductility, and work hardening characteristics of the constituents (fiber and matrix) as well as the characteristics of the interface. As mentioned above, conventional approaches to fatigue involve *S-N* curves and fatigue crack propagation studies. Another approach involves the monitoring of damage accumulation. Specifically, measurement of modulus loss as a function of cycles has been used extensively in polymer matrix and ceramic matrix composites (Chawla, K.K., 1997). In the following, we describe the fatigue behavior of continuous fiber reinforced MMCs.

8.1.1 Continuous Fiber Reinforced MMCs

Incorporation of fibers generally improves the fatigue resistance in the fiber direction. In general, in composites containing fibers aligned along the stress axis and in large volume fractions, high monotonic strength and modulus translates into high fatigue strength. This can be explained by the fact that with increasing stiffness and strength, an increasing fraction of the load is borne by the fibers. High strength, brittle fibers such as carbon or boron do not fatigue as readily as metals, although ceramic fibers have been shown to be susceptible to cyclic fatigue (Chawla et al., 2005; Kerr et al., 2005).

Typically, the *S-N* curves of fiber reinforced MMCs are close to horizontal. Figure 8.1 shows the *S-N* curves for unidirectionally reinforced 6061/B/40_f, Al/Al_2O_3(FP)/50_f, and Mg/Al_2O_3(FP)/50_f under tension-tension fatigue (Champion et al., 1978). The cyclic stress is normalized with respect to the ultimate tensile strength. The unidirectional MMCs show better fatigue properties than the matrix, when loaded parallel to the fibers. Note the rather flat *S-N* curves of all the composites. In unidirectional composites, the fatigue strength will be a maximum along the fiber direction, and the greatest efficiency will be achieved if the fibers have uniform properties, are as defect-free as possible, and are much stronger and stiffer than the matrix. McGuire and Harris (1974) observed that increasing the fiber volume fraction from 0 to 24% resulted in increased fatigue resistance of tungsten

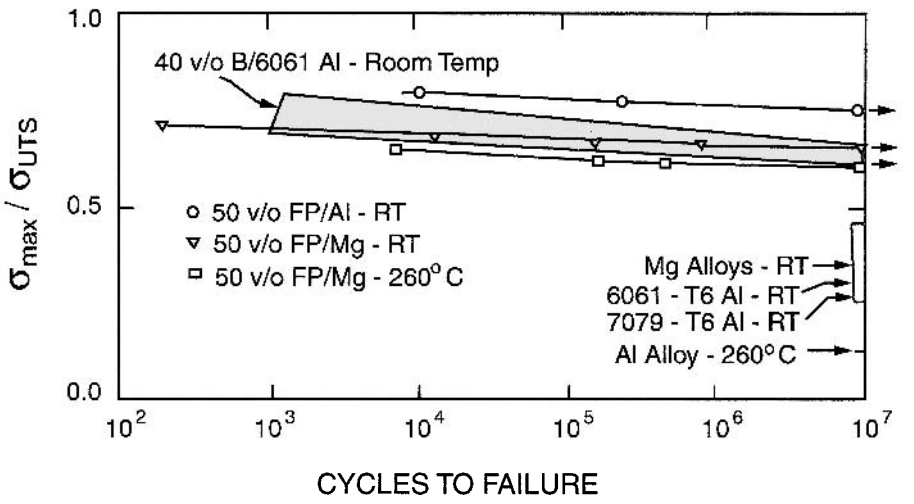

Fig. 8.1 Stress versus cycles (*S-N*) curves for unidirectionally reinforced 6061/B/40_f, Al/Al_2O_3(FP)/50_f, and Mg/Al_2O_3(FP)/50_f under tension-tension fatigue (after Champion et al., 1978). The fatigue strength of the composites is significantly enhanced over that of the monolithic alloys. FP is the Du Pont tradename for alumina fibers.

fiber reinforced Al-4Cu alloy under tension-compression cycling ($R = \sigma_{min}/\sigma_{max} = -1$). This was a direct result of increased monotonic strength and stiffness of the composite as a function of the fiber volume fraction. The enhancements in fatigue life due to increased stiffness of the composite are most pronounced in the HCF regime. Thus, in stress-controlled fatigue, for a given applied stress, the matrix in the composite will undergo a much lower strain than that of the unreinforced alloy.

Some work has been done to understand the fatigue damage mechanisms in continuous fiber reinforced MMCs. Baker et al. (1972) conducted one of the earliest studies on fatigue of continuous fiber reinforced MMCs. The *S-N* fatigue behavior of Al/B_f (125 μm fiber diameter) and Al/C_f (8 μm fiber diameter) composites was studied. The carbon fiber reinforced composites exhibited poor fatigue resistance, because of processing-induced fracture of the fibers and poor interfacial bonding. The following mechanisms were observed during fatigue: (a) fiber fracture dominated damage, where the rate of fiber fracture was much higher than cyclic plasticity in the matrix, and (b) matrix shear and plasticity induced localized and progressive fiber fracture. Mechanism (a) was shown to be predominant in low cycle fatigue, where the applied stresses were much closer to the ultimate strength of the fibers (and the composite). In high cycle fatigue, the fatigue damage in the composite is more likely to be controlled by matrix plasticity, followed by fiber fracture, or mechanism (b). Gouda et al. (1981) also observed crack initiation early in the fatigue life at defects in boron fibers in unidirectionally reinforced Al/B_f composites. These cracks then grew along the fiber/matrix interface and accounted for a major portion of the fatigue life, as would be the case in a composite with high fiber-to-matrix strength ratio. In composites with low fiber-to-matrix strength ratio, crack propagation may be a major portion of fatigue life, but the fatigue cracks grow through the fibers, resulting in poor fatigue resistance. Uniform spacing of fibers is also crucial, because clustered or touching fibers will result in enhanced stress concentration and easier crack nucleation.

The reader should note that because of the highly anisotropic nature of the fiber reinforced composites in general, the fatigue strength of off-axis MMCs, as in any fibrous composite, will be expected to decrease with increasing angle between the fiber axis and the applied stress axis. This has been confirmed by studies involving *S-N* behavior of alumina fiber reinforced magnesium composites (Hack et al., 1987; Page et al., 1987). It was found that the fatigue strength mirrored the tensile strength of the composites. Increased fiber volume fractions resulted in enhanced fatigue lifetimes in the axial direction, but little or no improvement was observed in the off-axis directions. Fatigue crack initiation and propagation occurred

primarily through the magnesium matrix. Thus, alloy additions to increase the strength of the matrix and fiber/matrix interface were incorporated. The alloy additions did improve the off-axis properties but decreased the axial properties. The reason for this was that while the alloy additions resulted in strengthening of the matrix and interface, they decreased the fiber strength.

Few direct microstructural observations of fatigue damage in continuous fiber reinforced MMCs have been conducted. One such study involved a single-crystal copper matrix containing tungsten fibers (Chawla, 1975). Tungsten/copper is an unusual metal matrix composite system. The two metals are mutually insoluble, yet molten copper wets tungsten. This allows for a strong mechanical bond between the tungsten fiber and the copper matrix, without any attendant chemical complications at the interface. The composites were made by liquid metal infiltration of fibers in vacuum. It was observed that the process of fabrication involving cooling from a temperature >1080°C (melting point of copper) to room temperature resulted in thermal stresses large enough to deform the copper matrix plastically (Chawla and Metzger, 1972). Dislocation etch-pitting technique was used to characterize the dislocation density in the single-crystal copper matrix. The dislocation density in the matrix was higher ($>10^8$ cm^{-2}) near the fiber/matrix interface than away from the interface. The dislocation distribution had a cellular structure, with the cell structure being better defined and smaller near the fiber than away from the fiber. This very heterogeneous distribution became homogeneous on cycling stress. The copper matrix structure after cycling had a high dislocation density distributed in a more or less uniform cellular structure.

Zhang et al. (2003) studied the *S-N* fatigue behavior of a 45 vol.% Nextel 610 alumina fiber reinforced pure Al matrix composite. The composite exhibited a tensile stress-strain behavior that was linear to failure, with about 0.7% strain-to-failure. In fatigue, the *S-N* curve was linear, with a fatigue strength (fatigue runout taken at 10^7 cycles) around 700 MPa. A clear and definitive fatigue strength was not apparent. The damage mechanisms varied considerably with applied stress. At very low stress (HCF regime), longitudinal cracking between fibers was the dominant failure mechanism, Fig. 8.2(a). It was suggested that these cracks initiated at fractured fibers and then grew parallel to the fiber direction. With increasing cyclic stress amplitude, in the intermediate regime between HCF and LCF, longitudinal matrix cracking was accompanied by transverse matrix cracks between fibers. Finally, at very high stresses (LCF regime), a single crack propagated in a catastrophic fashion perpendicular to the fibers, with no significant toughening, Fig. 8.2(b). Persistent slip band formation in the matrix has also

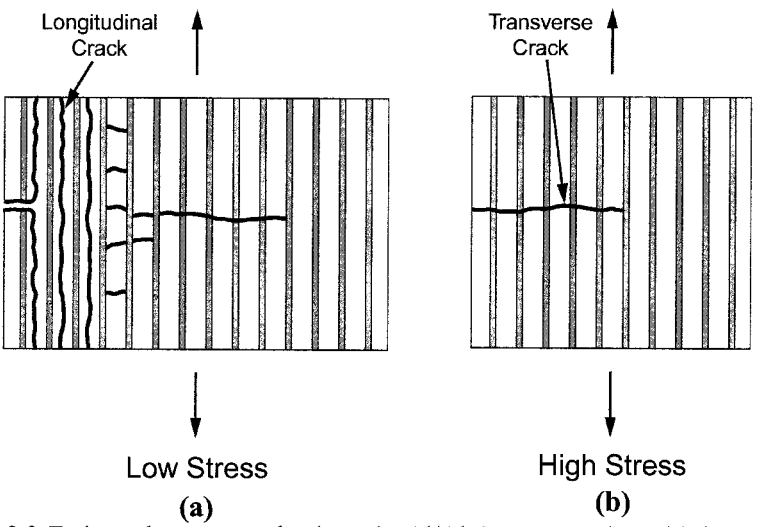

Fig. 8.2 Fatigue damage mechanisms in $Al/Al_2O_{3,f}$ composites: (a) low stress (high cycle fatigue), longitudinal splitting between fibers is the dominant failure mechanism and (b) high stress (low cycle fatigue), a single dominant crack propagates (after Zhang et al., 2003).

been shown to contribute to the development of fatigue cracks in the fibers, leading to fiber fracture (Majumdar and Newaz, 1995).

The fracture morphology is directly related to the fatigue regime of the material, i.e., crack velocity. Figure 8.3 shows the fracture surface of a SiC fiber reinforced Ti alloy matrix composite in the power law regime (also called the Paris regime) and in the fast fracture regime. In the Paris law regime, the localized fatigue striations are observed in the matrix of the composite. In the fast fracture region, the fracture is similar to that observed under monotonic tension, because of the very high crack velocities. Here, void nucleation and growth in the matrix are predominant, along with debonding at the fiber/matrix interface.

Finally, in composite systems where the interfacial bond strength is relatively weak, interfacial wear may contribute to fiber fracture. Interestingly, this behavior has been shown in ceramic matrix composites and can result in significant temperature rise of the composite at higher frequencies (>100 Hz), due to frictional heating (Chawla et al., 1996, Chawla, N., 1997). Walls and Zok (1994) quantified the extent of interfacial wear during fatigue in a fiber pushout test (see Chapter 4). The interfacial strength in the composite with increasing fatigue cycles was significantly lower than the as-received material, with a continuously increasing fiber displacement Fig. 8.4. This indicates that significant wear processes were taking place during fatigue (Walls et al., 1993). Figure 8.5 shows

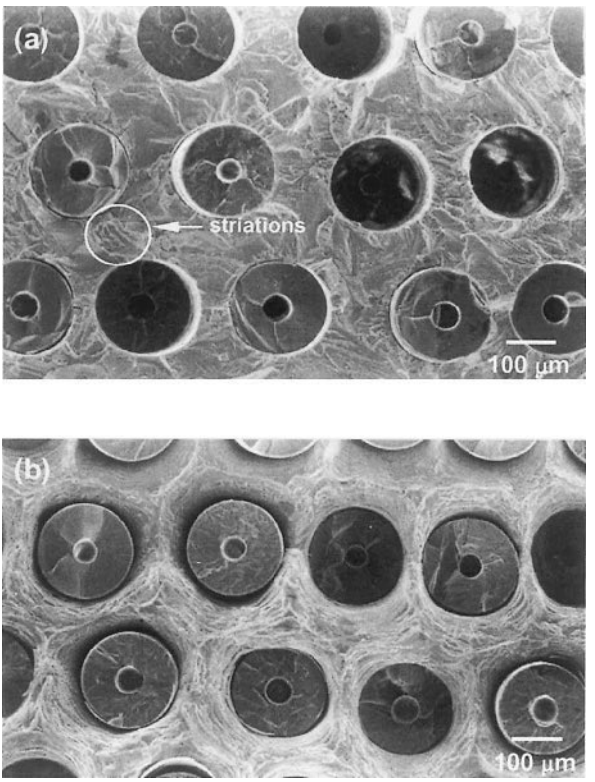

Fig. 8.3 Fatigue fracture in a Ti-β-21s/SiC_f(SCS-6) composite: (a) Paris law regime, showing localized striations in the matrix, and (b) fast fracture regime, where the matrix morphology is characteristic of void nucleation and growth (courtesy of J. Liu).

quantitative microstructural evidence of the interfacial wear process during fatigue of a Ti-β-21s (Ti-15Mo-2.7Nb-3Al-0.2Si)/SiC_f(SCS-6) composite obtained by *in situ* SEM (Liu and Bowen , 2003).

In addition to the mechanisms described above, elevated temperature also exacerbates fatigue damage. The mechanisms of fatigue damage are very much dependent on the composite system. In large-diameter SiC fibers (such as SCS-6), the surface of the fiber is C-rich. The fibers also contain a central carbon core. Thus, at elevated temperatures, the carbon will react with the matrix, such as Ti, to form hard and brittle carbides at the interface. The brittle carbides can act as fatigue crack initiation sites and catastrophic crack propagation can result. Foulk et al. (1998) also noted that oxygen dissolution of the interface combined with mechanical wear at the interface also degraded fatigue life. It was found that the stress on the fiber increased with

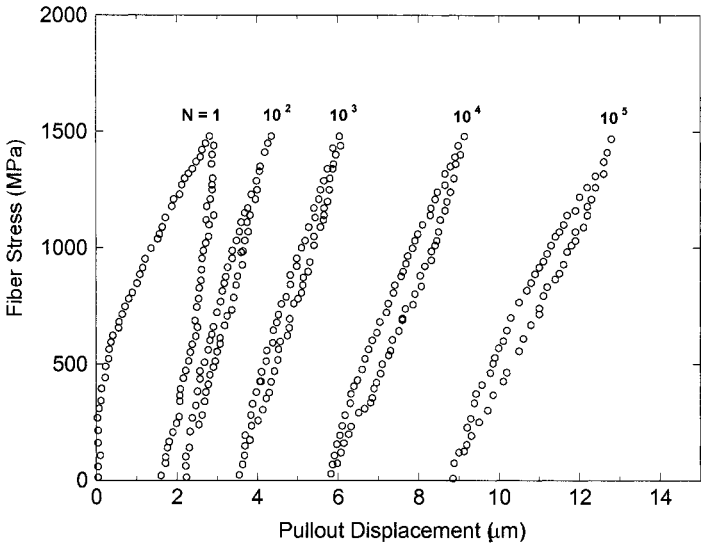

Fig. 8.4 Stress-strain hysteresis of a single fiber SiC fiber (SCS-6) in a Ti alloy matrix during fatigue. The hysteresis loops become wider with increasing cycles, indicating inelastic deformation in the form of wear at the fiber/matrix interface (after Walls and Zok, 1994).

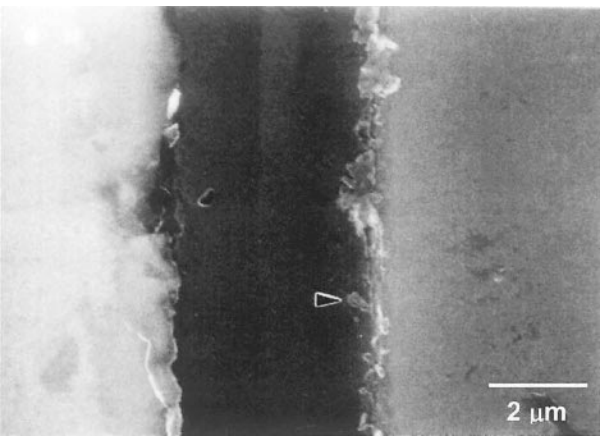

Fig. 8.5 In situ SEM micrograph of interfacial wear process during fatigue (indicated by arrow) of a Ti-β-21s/SiC_f(SCS-6) composite (courtesy of J. Liu).

increasing degradation of the interface. Significant degradation in interfacial shear strength, as measured by fiber pushout, due to interfacial wear and degradation due to elevated temperature fatigue has also been observed (Blatt et al., 1995). The fatigue damage is also controlled by cycling frequency. Lower frequencies allow more time for interfacial reaction to take

place, leading to lower fatigue lives (in cycles) in LCF, although in the HCF regime, the fatigue strength is about the same (Mall and Portner, 1992).

Sanders and Mall (1996) investigated the elevated temperature fatigue response (in strain control) of a Ti-15V-3Cr/SiC(SCS-6)/36_f in the transverse orientation. At relatively high strains, termed Region I, the composite had lower fatigue resistance than the matrix material, Fig. 8.6. This was attributed to matrix cracks, originating at the fiber/matrix interface, which resulted in premature failure of the composite, relative to the unreinforced alloy. With decreasing applied strain, Region II, the composite had equivalent transverse fatigue strength as the unreinforced alloy, although the damage mechanisms were quite different. In the monolithic alloy, creep-fatigue mechanisms took place. In the composite however, the interfacial damage took place which gradually progressed into matrix cracking. The matrix cracks, assisted by matrix creep, resulted in failure of the composite.

In non-structural composites, such as filamentary superconductor reinforced MMCs, the degradation of other functional properties is important. Salazar et al. (2004) studied the degradation in critical current density of a $Bi_2Sr_2Ca_2Cu_3O_x$(BSCCO)/Ag-Mg composite superconductor as a function of fatigue cycles at 77 K. Figure 8.7 shows the microstructure of the composite,

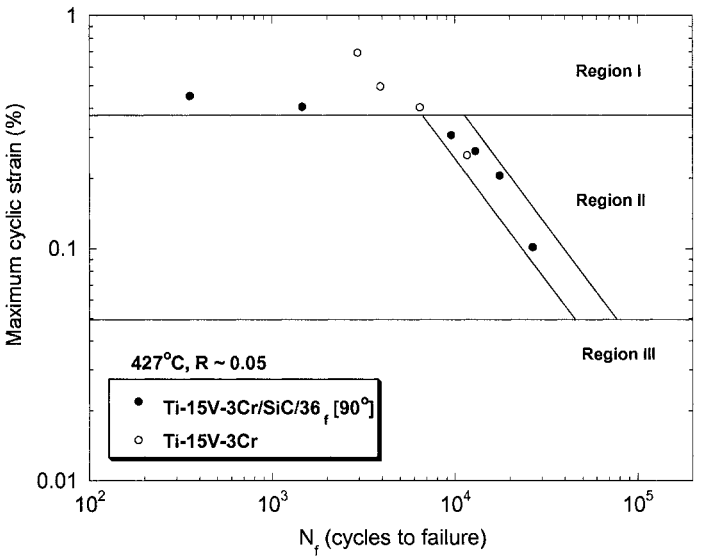

Fig. 8.6 Elevated temperature fatigue response (in strain control) of a Ti-15V-3Cr/SiC(SCS-6)/36_f in the transverse orientation. At relatively high strains, termed Region I, the composite has lower fatigue resistance than the matrix material. With decreasing applied strain, Region II, the composite has equivalent transverse fatigue strength as the unreinforced alloy (after Sanders and Mall, 1996).

which contains some processing-induced longitudinal cracks in the BSSCO filaments. An electric fatigue limit was defined, analogous to the mechanical fatigue limit, which corresponds to the stress below which degradation in electrical properties is negligible. In the BSSCO/Ag-Mg system, this corresponded to between 80-90% of the yield strength of the composites. Fracture of the ceramic superconductor filaments also took place during fatigue, eventually resulting in fatigue failure of the composite. Figure 8.8 shows fatigue microcracks that nucleated in the superconductor sheaths, which are not fully-dense. These cracks propagated until the superconductor/matrix interface was reached. Necking of the matrix between filaments occurred followed by fracture of the composite.

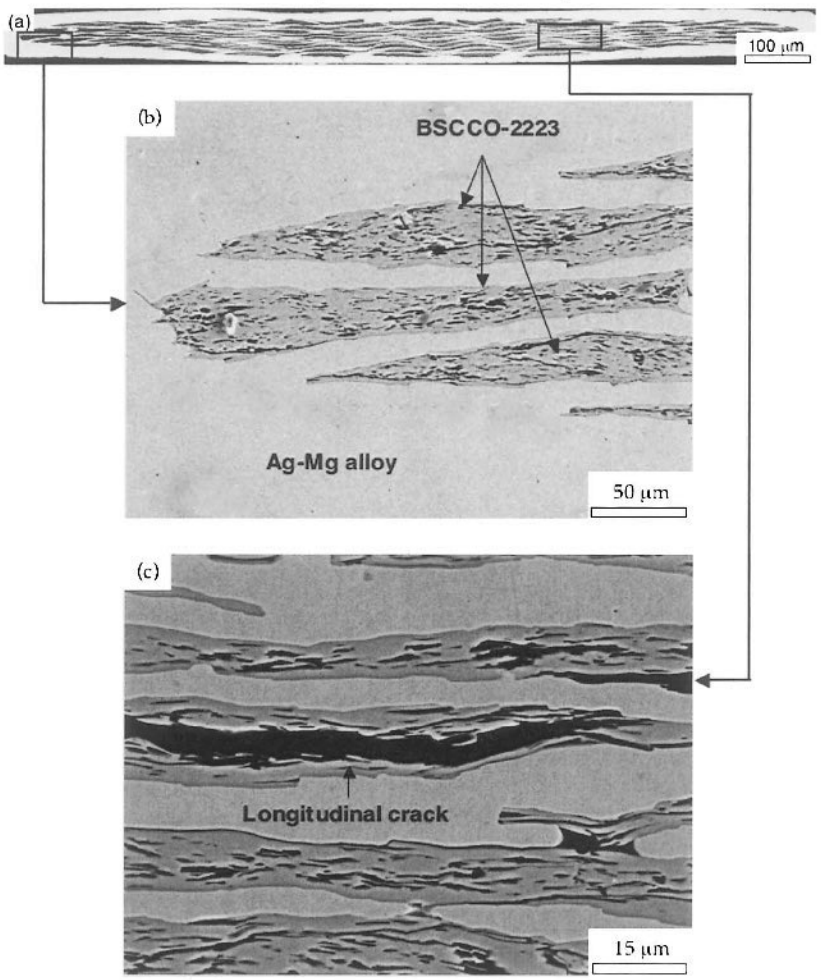

Fig. 8.7 Microstructure of $Bi_2Sr_2Ca_2Cu_3O_x$(BSCCO)/Ag-Mg composite superconductor (courtesy of J. LLorca). The BSSCO filaments contain some processing-induced longitudinal cracks.

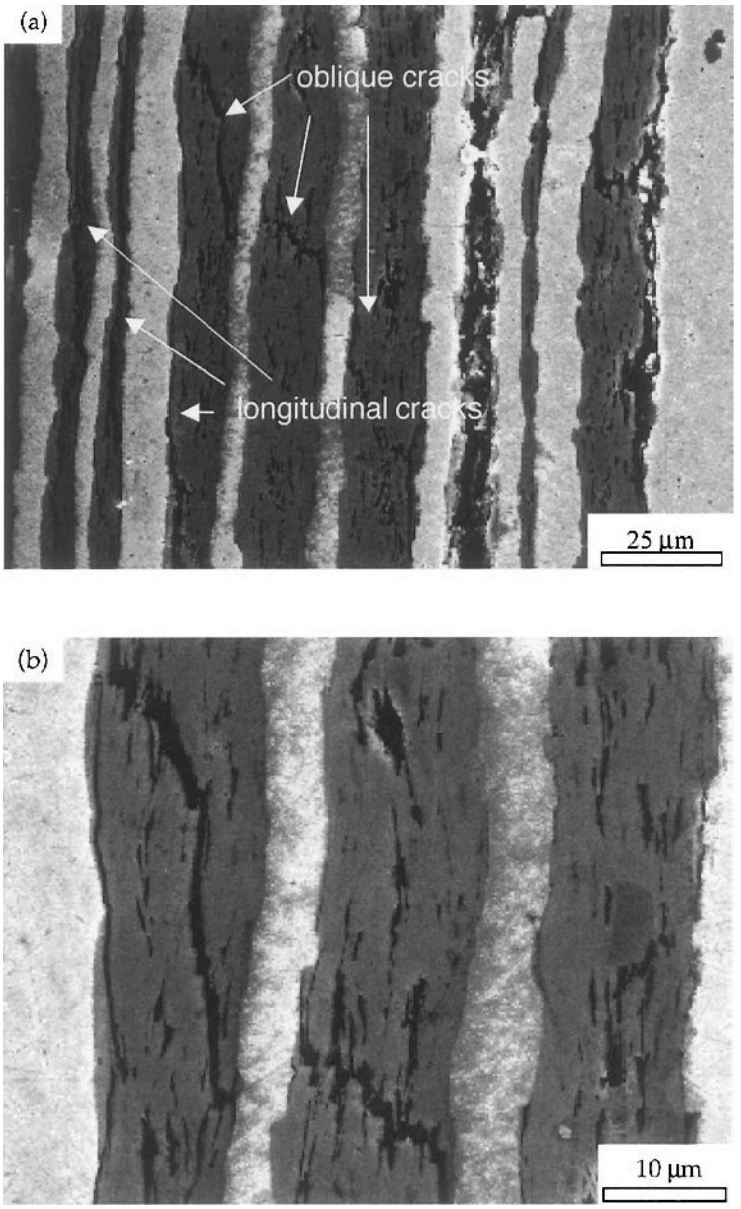

Fig. 8.8 Fatigue microcracks in $Bi_2Sr_2Ca_2Cu_3O_x$(BSCCO)/Ag-Mg composite superconductor: (a) lower magnification and (b) higher magnification (courtesy of J. LLorca). The cracks nucleate in the superconductor sheaths, which are not fully-dense. These cracks propagate until the superconductor/matrix interface is reached.

8.1.2 Stiffness Loss

The major problem in quantifying the stress intensity range during fatigue crack growth of fiber reinforced MMCs is the absence of *one and only* one dominant crack that is propagating. The lack of *self-similar* crack growth, i.e., when the crack propagates in the same plane and direction as the initial crack, is caused by the many modes of damage in MMCs, such as matrix cracking, fiber fracture, interfacial delamination and debonding, void growth, multidirectional cracking, and so on. These modes appear rather early in the fatigue life of composites. One manifestation of such damage is the stiffness loss as a function of cycles. In general, one would expect the scatter in fatigue data of composites to be much greater than that in fatigue of monolithic, homogeneous materials. This is because of the existence of a variety of damage mechanisms in composites. Thus, with continued cycling, there occurs an accumulation of damage. This accumulated damage results in a reduction of the overall stiffness of the composite. Measurement of stiffness loss as a function of cycling has been shown to be quite a useful technique of assessing the fatigue damage in polymer matrix composites (Chawla, 1997). In MMCs, the fatigue behavior of boron fiber and silicon carbide fiber reinforced aluminum and titanium alloy matrix composite laminates having different stacking sequences has been examined using the stiffness-loss measurement technique (Johnson, 1982; Johnson and Wallis, 1986; Johnson, 1988). It was observed that on cycling below the fatigue limit but above a distinct stress range, $\Delta\sigma$, the plastic deformation and cracking (internal damage) in the matrix led to a reduced modulus. Johnson (1988) has proposed a model that envisioned the specimen reaching a "saturation damage state" (SDS) during constant amplitude fatigue testing.

Gomez and Wawner (1988) also observed stiffness loss in silicon carbide/aluminum composites subjected to tension-tension fatigue (R = 0.1) at 10 Hz. The Young's modulus was measured at periodic intervals between cycles. The SCS coating fractured at high cycles, and the fracture surface showed the coating clinging to the matrix. Sanders and Mall (1996) also observed a distinct decrease in Young's modulus and maximum stress under strain-controlled fatigue of Ti-15V-3Cr/SiC(SCS-6)36_f, under transverse loading, Fig. 8.9. Two distinct stages of damage were observed. In stage I, the damage in modulus and stress was relatively stable. In stage II, however, significant damage, likely due to interfacial fracture, resulted in a significant decrease in the Young's modulus and the stress carried by the composite.

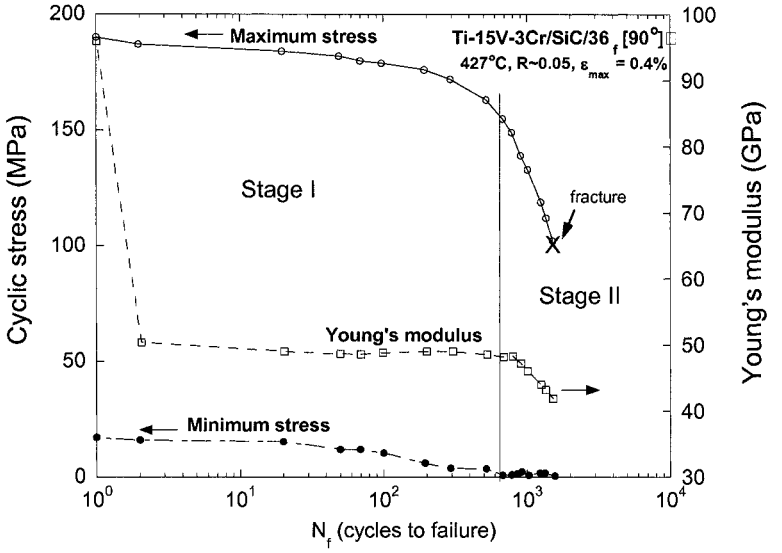

Fig. 8.9 Decrease in Young's modulus and maximum stress in strain-controlled fatigue of Ti-15V-3Cr/SiC(SCS-6)36_f, under transverse loading (after Sanders and Mall, 1996). In stage I, the damage in modulus and stress is relatively stable. In stage II, however, significant damage, likely due to interfacial fracture, resulted in a significant decrease in the stress carried by the composite and the Young's modulus.

8.1.3 Particle Reinforced MMCs

The use of a high stiffness ceramic reinforcement in particulate form can result in a substantial increase in fatigue resistance while maintaining cost at an acceptable level. The fatigue resistance of particulate MMCs depends on a variety of factors, including reinforcement particle volume fraction, particle size, matrix and interfacial microstructure, the presence of inclusions or defects that arise from processing, and testing environment (Chawla and Shen, 2001; Chawla and Allison, 2001; Lewandowski, 2000; LLorca, 2002; Ganesh and Chawla, 2004). The effect of these factors on the fatigue behavior of particle reinforced MMCs is summarized in this section.

Several studies have shown that increasing volume fraction and decreasing particle size both result in enhanced fatigue resistance (Hall et al., 1994; Poza and LLorca, 1999; Chawla et al., 1998a; Chawla et al., 2000a; Chawla et al., 2000b). In the composite, most of the load is carried by the high modulus, high strength reinforcement, so for a given stress, the composite undergoes a lower average strain than the unreinforced alloy. Thus, the fatigue lives of particle reinforced metal matrix composites are generally superior to those of unreinforced metals, Fig. 8.10. These improvements are

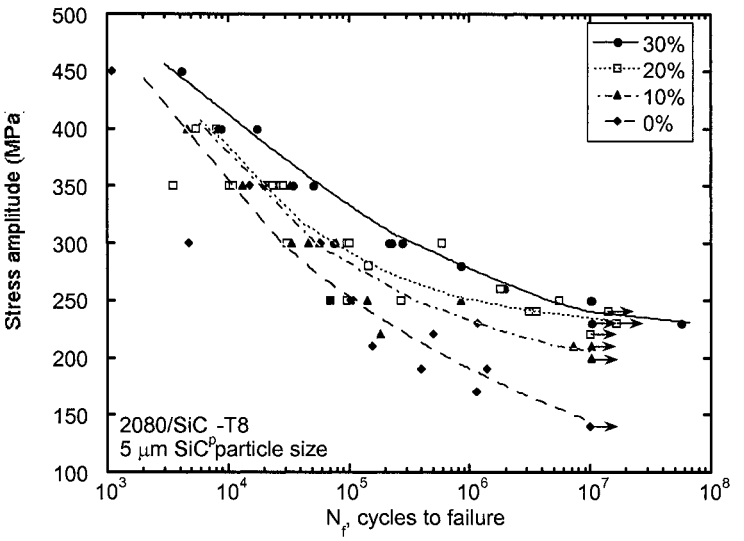

Fig. 8.10 Effect of SiC volume fraction on the stress versus cycles fatigue behavior of 2080 Al/SiC_p composites. Increasing volume fraction results in higher fatigue life (after Chawla et al., 1998).

most pronounced at low cyclic stresses, i.e., in the high cycle fatigue regime, while at higher cyclic stresses the differences between reinforced and unreinforced materials are reduced. This is called "ductility exhaustion" of the composites, which takes place in the low cycle fatigue regime. The higher ductility of the unreinforced alloy in this regime contributes to higher fatigue life than that of the composite. With decreasing particle size, for a given reinforcement volume fraction, the reinforcement interparticle spacing decreases, resulting in more barriers to the reversible slip motion that takes place during fatigue, and a decrease in strain localization by cyclic slip refinement. Above a critical particle size, reinforcement fracture is predominant and contributes to a low fatigue life, because of the increased propensity for particle cracking as the particle size increases (Chawla et al., 1998a). Narrowing of the particle size range distribution also results in higher fatigue life, particularly when eliminating larger particles that are more prone to cracking (Couper and Xia, 1991).

The cyclic stress-strain behavior of the composite is also affected by the onset of microplasticity at relatively low stress (see chapter 7). Chawla et al., (1998b) compared the cyclic stress-strain behavior of a 2080/SiC/30_p composite with that of the unreinforced alloy. The composite exhibited microplasticity at relatively low stresses, presumably due to stress concentrations at SiC particles and localized plasticity at the poles of the reinforcement, 8.11(a). The cyclic stress-strain curve of the 2080 Al alloy at

the same stress was elastic in nature, although it was more compliant than the composite. At an applied stress higher than the yield strength of the unreinforced alloy, the hysteresis loop for the unreinforced alloy was much larger than that of the composite, 8.11(b). It should be noted that the onset of cyclic microplasticity in the composite at low stress did not appear to affect the fatigue life of the composite in a detrimental fashion. Rather, the composites had higher fatigue life than the unreinforced alloy. Chawla and Shen (2001) used a unit cell finite element model, consisting of spherical particles arranged in a staggered arrangement, shown in the inset of Fig. 8.12. The cyclic stress-strain hysteresis obtained from this simple model yielded surprisingly good agreement with the experimental behavior, see Fig. 8.12. The effects of reinforcement aspect ratio, shape, and matrix hardening characteristics on cyclic fatigue have also been elucidated (LLorca et al., 1992; LLorca, 1994).

The cyclic stress-strain behavior of MMCs is also affected by a phenomenon called the Bauschinger effect. The Bauschinger effect is defined as a decrease in flow stress that occurs when we reverse the loading direction, e.g., from a tensile to compressive stress or vice versa (Bauschinger, 1886). Thus, an understanding of the Bauschinger effect is essential to understanding of work hardening and cyclic loading.

One of the origins of the Bauschinger effect in monolithic materials has been attributed to dislocation pileup. Pileup of dislocations, in the forward loading direction, creates a "back-stress" which aids deformation upon reversal in loading, resulting in a lower flow stress (Mott, 1952; Seeger et al., 1958). In precipitation-hardened materials, Orowan loops associated with the precipitate particles also induce a back-stress (Orowan, 1959). The phenomenon has also been observed in particle reinforced MMCs (Arsenault and Wu, 1987; LLorca et al., 1990). Here, the back-stress is enhanced by tensile residual stresses that are generated upon cooling from the processing temperature, as well as constrained deformation of the matrix by the rigid particles. This results in a loading asymmetry (Arsenault and Wu, 1987; Arsenault and Pillai, 1996) where a more significant Bauschinger effect was observed under compression-tension sequence than for a tension-compression sequence.

Indeed, finite element modeling shows that even when the matrix is assumed to exhibit isotropic hardening behavior (i.e., no Bauschinger effect exists), the composite shows a distinct Bauschinger effect upon reversed loading (LLorca et al., 1990), as was observed experimentally. An examination of the evolution of local stress field showed an apparent early reversed yielding for the composite, due to non-uniformity of deformation in the matrix caused

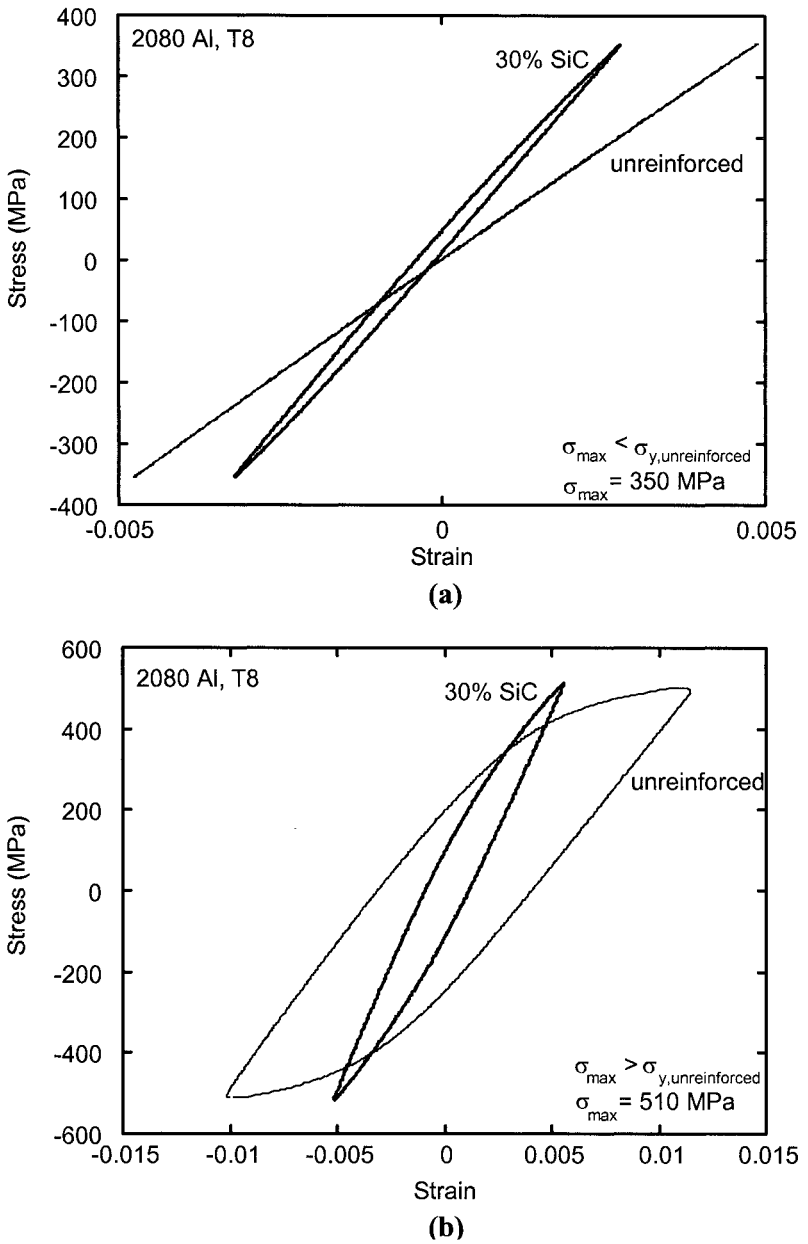

Fig. 8.11 Comparison of cyclic stress strain behavior of a 2080/SiC/30p composite and 2080 Al unreinforced alloy (Chawla et al., 1998b): (a) low cyclic stress ($\sigma_{max} < \sigma_{y,unreinforced}$), and (b) high cyclic stress ($\sigma_{max} > \sigma_{y,unreinforced}$). The composite exhibits microplasticity at very low stress, due to localized plasticity at the poles of the SiC reinforcement and at sharp particle corners.

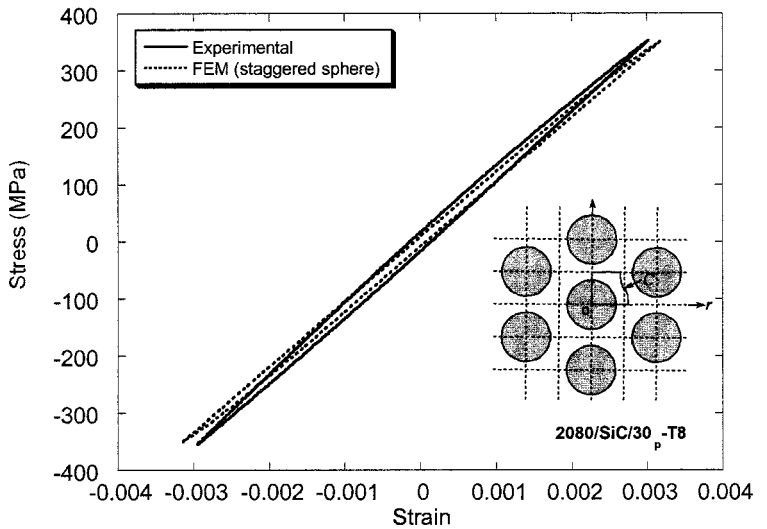

Fig. 8.12 Cyclic stress-strain hysteresis behavior of a 2080/SiC/30_p composite (after Chawla and Shen, 2001). A finite element model consisting of spherical, staggered SiC particles in Al predicts the experimental behavior very well.

by the constraint imposed by the brittle reinforcement (Shen et al., 1995). Thus, high *local* effective stresses trigger early *local* yielding after the load is reversed, which is reflected in the macroscopic stress-strain behavior.

In addition to particle reinforcement, the matrix microstructure also significantly influences the fatigue behavior of the composite. Factors affecting the matrix microstructure include size, shape, and spacing of precipitates, grain size, and non-reinforcement dispersoids or inclusions (such as Fe-rich inclusions in aluminum that are commonly formed during processing). It would appear that with regard to grain size, composites follow the same trend as monolithic materials, i.e., for a given matrix alloy composition and volume fraction of reinforcement, finer grain sizes generally result in improved properties. Contrary to conventional wisdom for monolithic materials, in MMCs high matrix yield and ultimate tensile strength do not necessarily reflect high fatigue strength (defined here as fatigue runout at 10^7 cycles). Vyletel et al. (1991) showed that there was no significant difference in fatigue behavior between naturally aged and artificially aged MMC, even though the naturally aged material had a much lower yield and ultimate strength. Chawla et al. (2000b) compared two materials with constant reinforcement volume fraction and particle size, but very different microstructures. A thermomechanical treatment (T8) of the Al-Cu-Mg alloy produced a fine and homogeneous distribution of S' precipitates, while a thermal treatment only (T6) resulted in coarser and

inhomogeneously distributed S' precipitates. Because of finer and more closely spaced precipitates, the composite that underwent a T8 treatment exhibited higher yield strength than the T6 material. Despite its lower yield strength, however, the T6 matrix composites exhibited higher fatigue resistance than the T8 matrix composites. This contrasting behavior between monotonic and cyclic loading can be attributed to the strong influence of the presence, stability, and morphology of the S' precipitates in the matrix of the composite (Calabrese and Laird, 1974a; Calabrese and Laird, 1974b; Starke and Luetjering, 1979). In fatigue, failure processes are affected by a variety of microstructural factors, which include resistance to dislocation motion and possible dislocation pileup at precipitates and/or reinforcement particles and cracking along slip bands. In aluminum alloys, small precipitates with a coherent interface are easily sheared (Calabrese and Laird, 1974a; Calabrese and Laird, 1974b). Coarser precipitates, which have a semi-coherent or incoherent interface with the matrix, cause the dislocation to loop around the precipitate. In the T8 materials, the precipitates are fine enough that it is believed that the precipitates are cut by dislocations and precipitate slip bands (PSBs) are formed during fatigue, which reduces the strengthening effect of precipitates, thereby impairing the fatigue strength. In the T6 materials, the larger precipitate size allows them to retain their precipitates structure and strength during fatigue.

Overaging heat treatments also modify the matrix microstructure, resulting in coarsening of the precipitate structure, while retaining a homogeneous precipitate distribution, which directly influences fatigue life (Chawla et al., 2000b). Figure 8.13 shows the coarsening and increase in precipitate spacing in the matrix of MMCs overaged at various temperatures for 24 hours. Increasing precipitate spacing decreases both fatigue strength and fatigue lifetime, Fig. 8.14. This is to be expected since coarser precipitates result in a larger interprecipitate spacing and easier bypass of dislocations. For the composites subjected to higher overaging temperatures, the yield strength and fatigue strength also decrease with increasing precipitate spacing. It is important to realize that precipitate size alone should not be taken as the determining factor for fatigue resistance. Rather, the precipitates should be of sufficient size not to be susceptible to precipitate shearing, but should be semi- or completely coherent with the matrix to impede dislocation motion.

Processing-related defects in the form of intermetallic inclusions or particle clusters are also part of the matrix microstructure, and can play a role in fatigue strength, particularly in powder metallurgy processed materials (Chawla et al., 1998a; Chawla et al., 2000a; Li and Ellyin, 1996). Figure 8.15 shows a fracture surface of a 2080/SiC/20_p composite (Chawla et al., 1998a). The crack initiates at an Fe-rich inclusion. This is followed by a

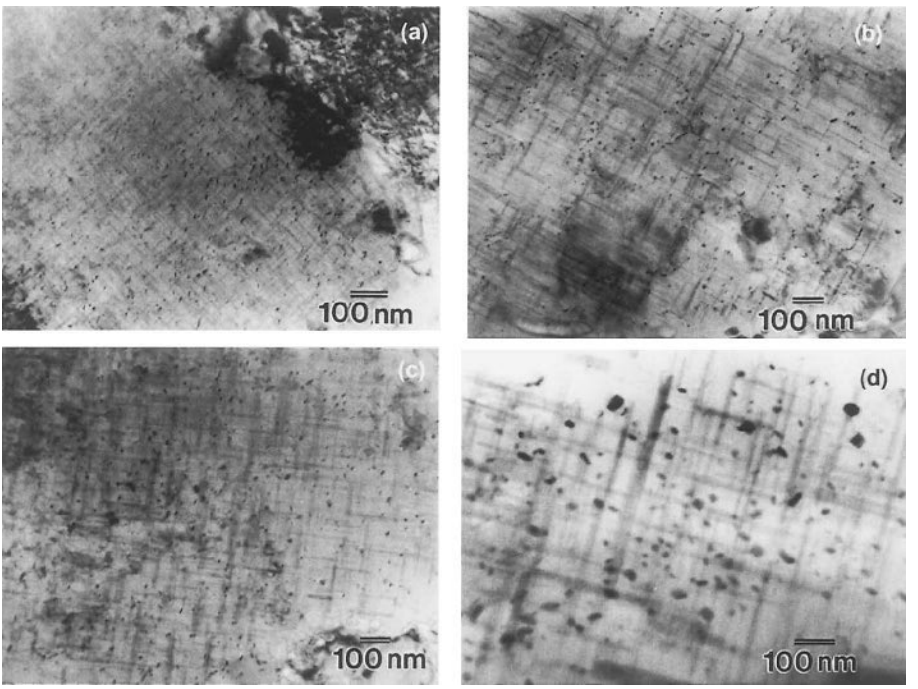

Fig. 8.13 Coarsening of S' precipitates due to overaging: (a) solution treated, rolled, and aged (T8), (b) T8+24 h at 200°C, (c) T8+24 h at 225°C, and (d) T8+24 h at 250°C (Chawla et al., 2000a).

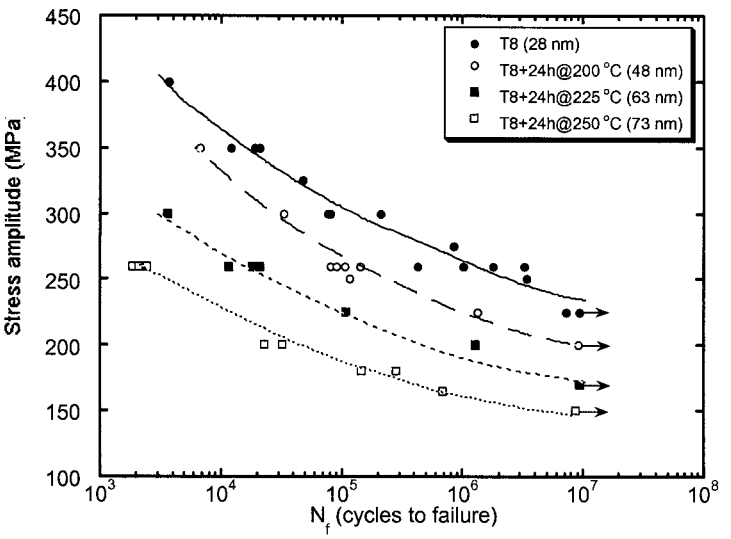

Fig. 8.14 Influence of matrix precipitate spacing on fatigue life of 2080/SiC/20_p-T6 composite. Increase in precipitate spacing results in a reduction in fatigue life (after Chawla et al., 2000a).

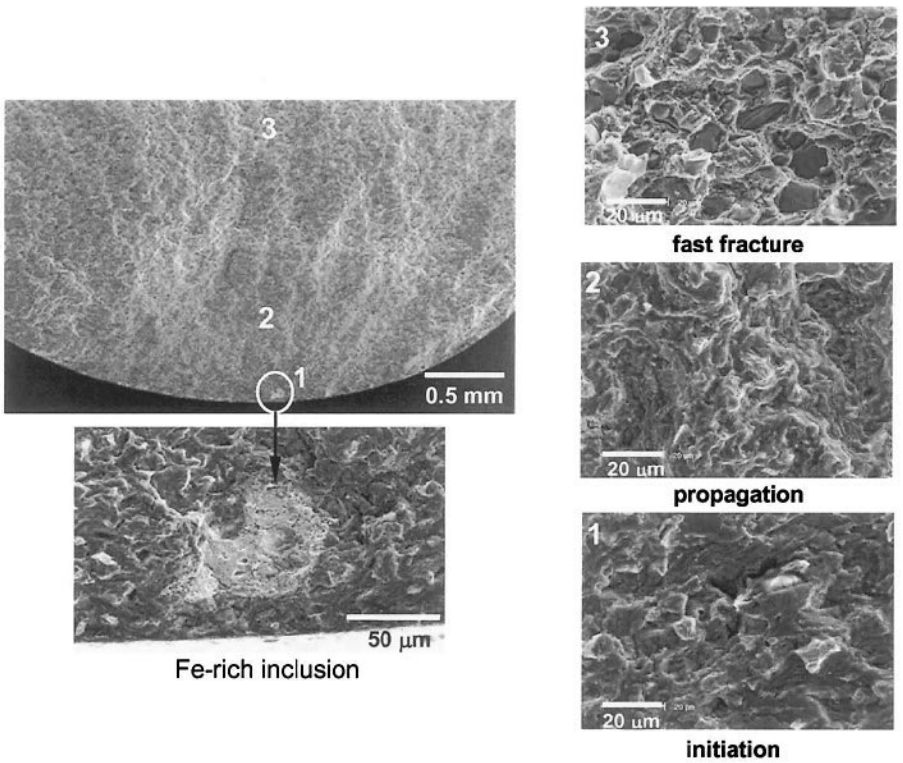

Fig. 8.15 Fatigue fracture morphology in a 2080/SiC/20_p-T6 composite consisting of initiation, propagation, and fast fracture regions (after Chawla et al., 1998a).

region of stable crack propagation, followed by fast-fracture. The last stage is characterized by a large amount of particle fracture, due to the high crack velocity. The defects (e.g., inclusions, particle clusters) act as stress concentrators and increase the local stress intensity in the material, promoting easy crack nucleation. For a given inclusion size, the stress concentration in a composite, where the inclusion is surrounded by high stiffness reinforcement particles, is lower than in the unreinforced alloy. Since more of the load is being "shared" by the high stiffness SiC particles in the composite, an inclusion in the composite will be subjected to lower stress than a similar inclusion in the unreinforced alloy.

In extruded composites, the overall size of inclusions is also lower since the ceramic reinforcement particles break the brittle inclusions into smaller sizes during extrusion, Fig. 8.16, (Chawla et al., 2000a). It is interesting to note that in the low cycle regime, cracks seem to originate relatively early in fatigue life (around 10% of total life) (Chawla et al., 1998a; Lukasak and

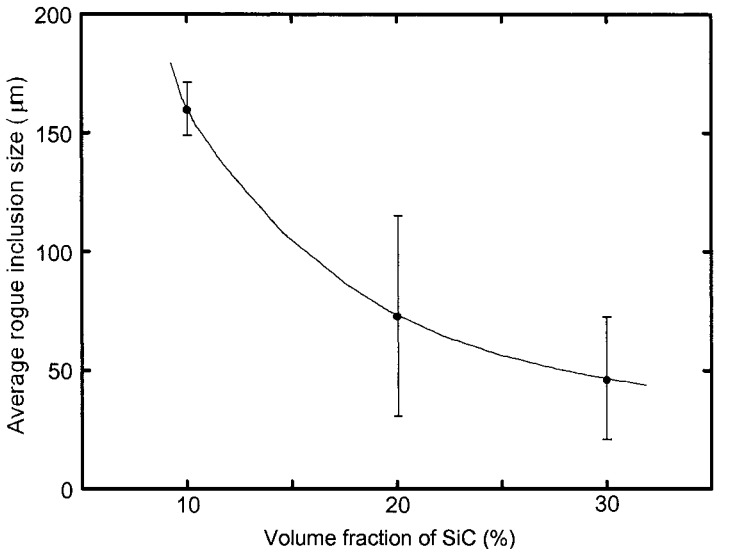

Fig. 8.16 Average "rogue inclusion" size as a function of SiC particle volume fraction. The hard particles contribute to the beneficial fracture and comminution of the Fe-rich inclusions during processing (after Chawla et al., 2000b).

Koss, 1993). In the high cycle regime, on the other hand, crack initiation can occur quite late (after about 70-90% of the life of the specimen). While crack growth is relatively unimpeded in unreinforced materials, crack growth is hindered by mechanisms such as crack deflection and crack trapping in the composite. A more detailed discussion of crack growth in these materials is given in the next section.

Several MMC applications require fatigue resistance at elevated temperatures (on the order of 150-175°C). Figure 8.17 shows the elevated temperature fatigue performance of MMCs in comparison with the room temperature data shown in Fig. 8.10 (Chawla et al., 1999). The most significant debit in fatigue strength occurred between 25 and 150°C. The incremental increase in temperature to 170°C resulted in a modest decrease in fatigue strength. In applications where elevated temperature fatigue resistance is a criterion, the temperature at which the composite is aged also becomes very important. At temperatures slightly higher than the aging temperature, a severe decrease in fatigue strength may take place because of significant matrix overaging. The fatigue strength in the composites seems to be directly proportional to the strength of the matrix, although the decrease in fatigue strength due to temperature is significantly higher than the decrease in yield strength. This may be caused by changes in matrix microstructure and decrease in matrix strength from a combination of long-term exposure and cyclic stress. The fatigue fracture morphology after

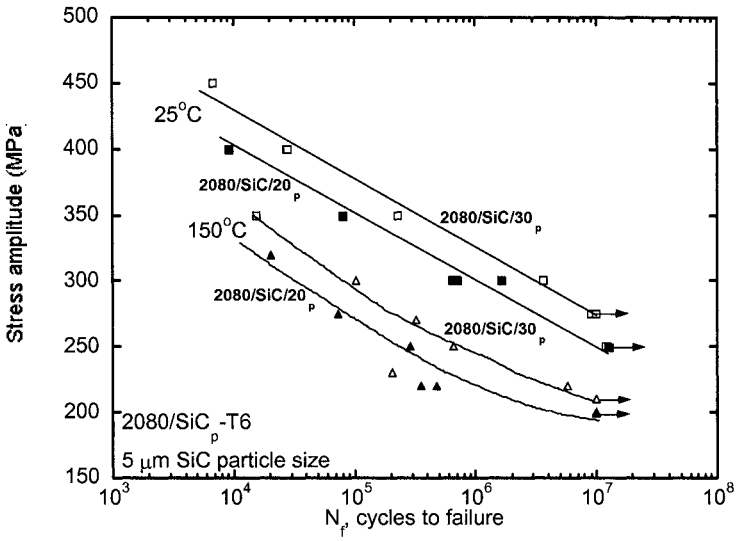

Fig. 8.17 Elevated temperature fatigue of 2080/SiC_p composites. A slight decrease in fatigue resistance is observed at elevated temperature (after Chawla et al., 1999).

elevated temperature fatigue is quite different from that at room temperature. At elevated temperature, while crack initiation takes place at the inclusions, fractography also indicates evidence of interfacial decohesion and void growth at the particle/matrix interface and particle corners, as well as in the matrix of the composite, Fig. 8.18. It appears that microvoid nucleation and coalescence in the matrix have also taken place prior at fracture.

Temperatures during metal cutting can rise to as much 1200°C (Kindermann et al., 1999). Tungsten carbide/cobalt composites, commonly referred to as cemented carbides or hardmetal, are used for cutting a range of materials under environments involving aggressive chemicals, high-temperatures, lubricants, and water-based coolants. Cyclic fatigue behavior of such materials is of importance because cyclic loading in these materials occurs during the alternating slip and stick of the metal chips during machining, vibrations of the machines, and the interrupted cutting process (Almond and Roebuck, 1980; Roebuck et al., 1984; Kindermann et al., 1999; Pugsley and Sockel, 2004). An example of an S-N curve for WC/6 wt.% Co composite in air and tannic acid (to simulate wood cutting) is shown in Fig. 8.19. The evidence of corrosion fatigue effect at low stress amplitudes is clear. Figure 8.20 shows a strong decrease in fatigue behavior at 700°C vis-à-vis room temperature. Also shown in the figure are the inert strength values of these composites, which are significantly higher than the cyclic strength values at all cycles. This indicates the loss of strength is not due to surface oxidation

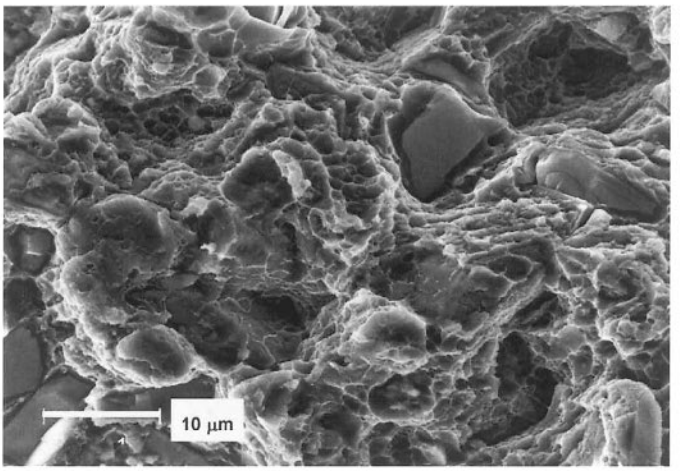

(a)

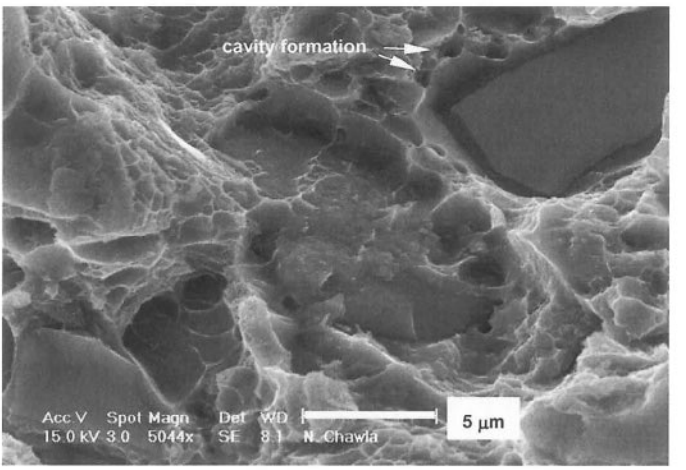

(b)

Fig. 8.18 Elevated temperature fatigue fracture morphology, showing (a) dimpled fracture and interfacial decohesion and (b) cavity formation in the matrix (after Chawla et al., 1999).

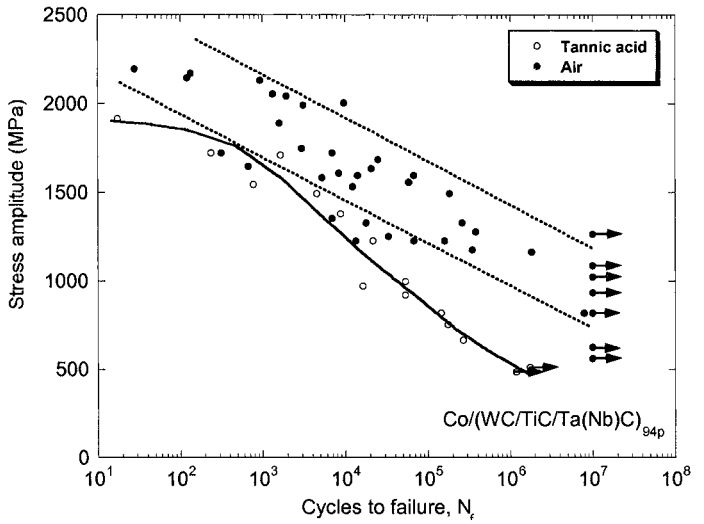

Fig. 8.19 S-N curve for WC/Co composites in air and in tannic acid at 4 Hz (after Pugley and Sockel, 2004). The effect of corrosion fatigue effect, at low stress amplitudes, is clear.

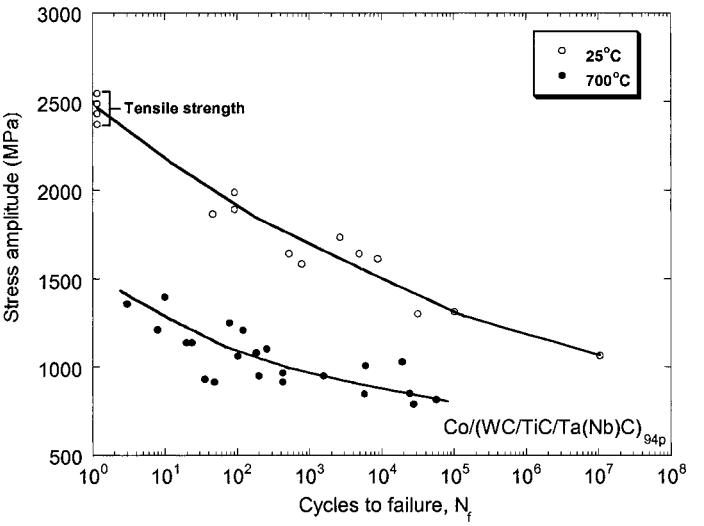

Fig. 8.20 S-N curves for WC/Co composites at room temperatures and at 700°C (after Kindermann et al., 1999).

of WC at high temperatures but a true high-temperature cyclic fatigue phenomenon.

8.2 FATIGUE CRACK GROWTH

In this section, we describe the fatigue crack growth behavior of MMCs. A brief summary of the salient features of fatigue crack growth in engineering materials, including a description of fatigue crack closure and the two parameter approach to fatigue, is given in an inset.

8.2.1 Continuous Fiber Reinforced MMCs

In general, the fibers provide a crack-impeding effect, but the nature (morphology, rigidity, and fracture strain) of the fiber, the fiber/matrix interface, and/or any reaction-zone phases at the interface can have a great influence on fatigue crack growth processes (Chawla, 1991). In composites with a relatively high interface strength, the fatigue crack propagates straight through the fibers, Fig. 8.21(a). With a weak interface, fiber/matrix debonding, crack deflection, fiber bridging, and fiber pullout take place, Fig. 8.21(b) and 8.22. This leads to a significant amount of energy-dissipation during crack growth which results in macroscopic toughening of the composite.

In general, fiber reinforced MMCs exhibit superior fatigue crack growth resistance to monolithic alloys. An example is the case of boron fiber (coated with B_4C) reinforced Ti-6Al-4V composite and the parent matrix alloy, shown in Fig. 8.23 (Harmon et al., 1987). Note that the MMC has a higher fatigue threshold and a much lower rate of crack growth through most of the fatigue life. Soumeldis et al. (1986) observed lower fatigue-crack growth

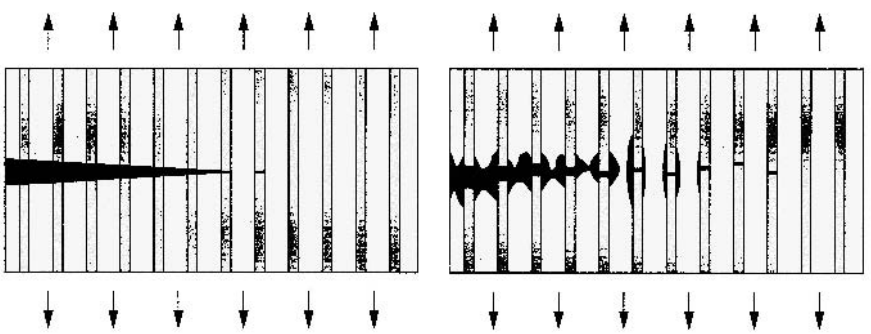

Fig. 8.21 Schematic of damage mechanisms in continuous fiber reinforced MMCs: (a) strong interface – fatigue crack propagates straight through the fibers; and (b) weak interface – fiber/matrix debonding, crack deflection, fiber bridging, and fiber pullout take place.

Fatigue Crack Growth in Engineering Materials

As described in the beginning of the chapter, the fatigue crack growth behavior of engineering materials is characterized by a plot of log da/dN versus log ΔK.. A three-region curve is obtained. Regime 1 is often denoted as the threshold regime, to indicate a threshold stress intensity factor, ΔK_{th} (typically corresponding to $\sim 10^{-10}$ m/cycle), for crack growth. With increasing ΔK, a linear portion on the log-log plot is observed, which is called the Paris regime. At even higher ΔK, the crack growth rate increases rapidly, resulting in fracture of the material.

In order to fully understand the crack growth behavior, let us define some important parameters. The nominal cyclic stress intensity factory range, ΔK, is equal to:

$$\Delta K = K_{max} - K_{min}$$

where K_{max} and K_{min} are the maximum and minimum stress intensity factors, respectively, obtained from the maximum and minimum applied stress, σ_{max} and σ_{min} and the corresponding crack lengths.

Fatigue Crack Closure

During the cyclic process, premature "closure" of the crack may take place, at a stress intensity value before reaching K_{min}. Crack closure during fatigue has been attributed to many origins, including plasticity at the crack tip, oxidation, crack surface roughness, and by wedging of asperities in the crack mouth. These are shown in the figure on the following page.

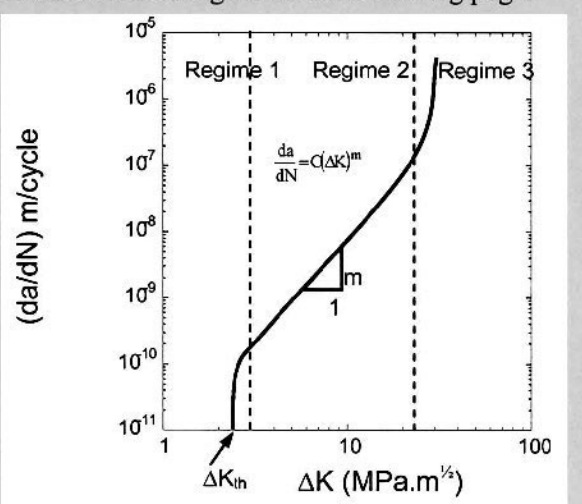

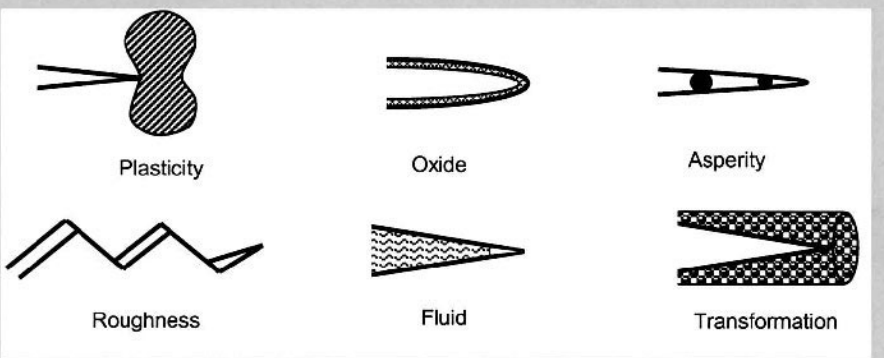

Because of premature closure of the crack faces, the driving force for crack growth is smaller than ΔK. Thus, we define an additional parameter, which corresponds to the stress intensity factor required to open the crack or K_{cl}. Now, the *effective* stress intensity factor, ΔK_{eff} (as shown schematically below), is given by:

$$\Delta K_{eff} = K_{max} - K_{cl}$$

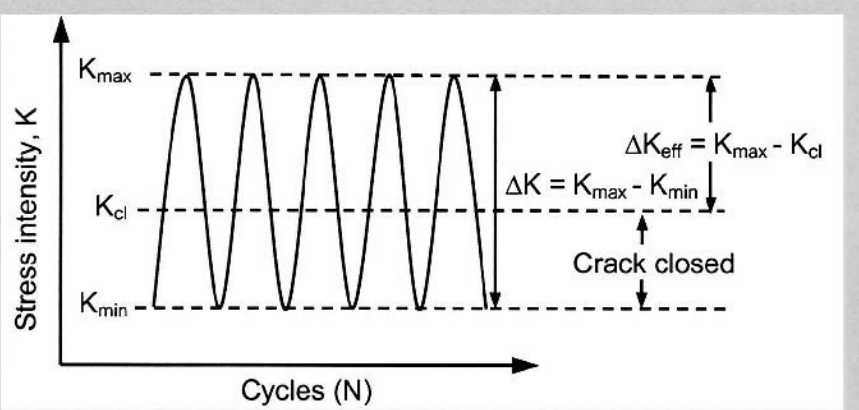

Two-Parameter Approach to Fatigue

Fatigue crack growth behavior can also be analyzed using a two-parameter approach (Doker and Marci, 1983; Vasudevan et al., 1994). The basis of this analysis is that there are two driving forces for fatigue crack growth: (a) static parameter or K_{max} and (b) cyclic parameter or ΔK. By conducting experiments at several R-ratios (K_{min}/K_{max} or $\sigma_{min}/\sigma_{max}$), the ΔK_{th} is obtained for a range of K_{max}. By plotting ΔK_{th} versus K_{max}, an 'L' shaped curve is obtained. The vertical and horizontal asymptotes of the curve correspond to ΔK^*_{th} and K^*_{max}. The physical meaning of these two parameters is that

critical values of both the static and cyclic driving forces must be met *simultaneously* for fatigue crack growth to take place. This is shown by the shaded region in the curve.

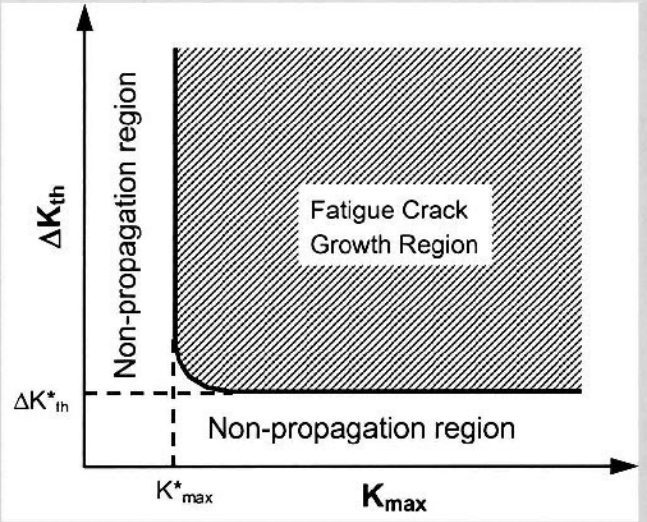

Using the two-parameter analysis, several important materials can be subdivided into different classes (Vasudevan and Sadananda, 1995). It is shown that environmental effects also play an important role on fatigue crack growth behavior.

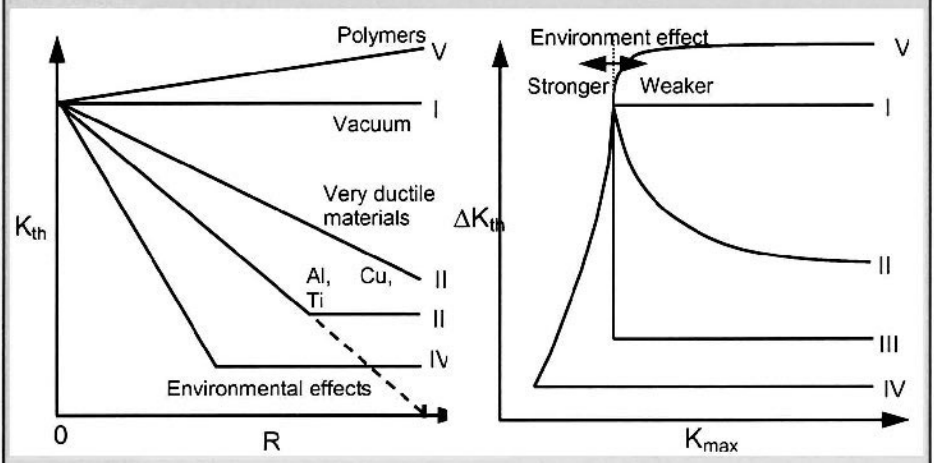

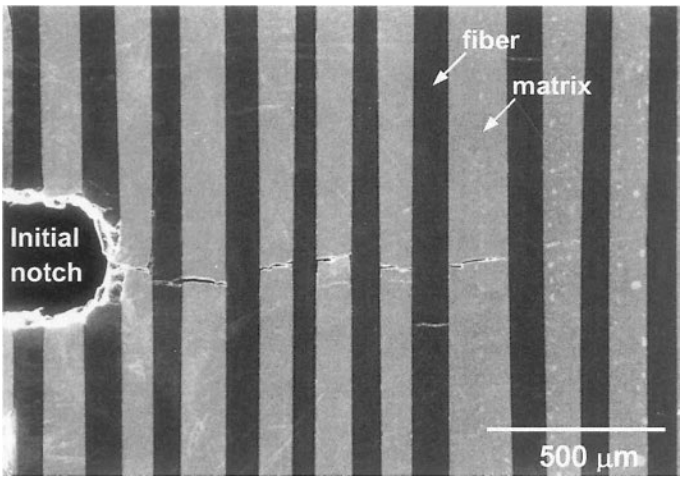

Fig. 8.22 Fatigue crack growth in a Ti-β-21s/SiC_f (SCS-6) composite exhibiting interfacial debonding, crack deflection, and fiber bridging (courtesy of J. Liu).

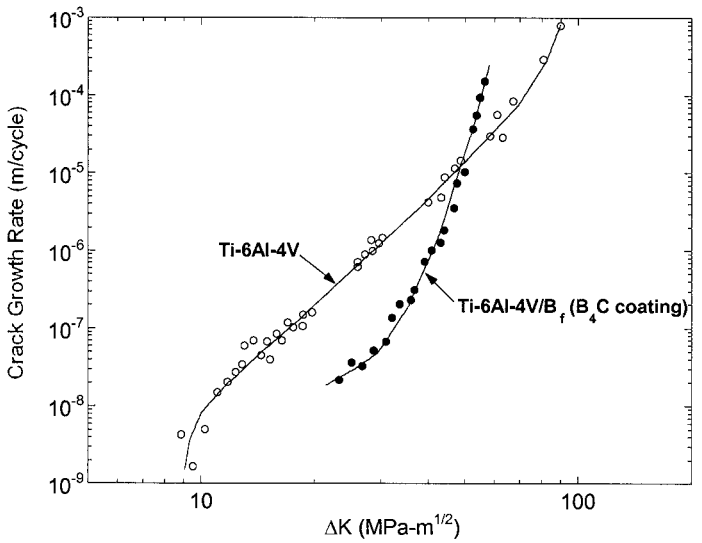

Fig. 8.23 Fatigue crack growth behavior of a boron fiber (coated with B_4C) reinforced Ti-6Al-4V composite and the parent matrix alloy (after Harmon et al., 1987). The fiber reinforced MMC has superior fatigue crack growth resistance to the monolithic alloy.

rates in fiber reinforced Ti-6Al-4V compared with that in the unreinforced alloy. Long isothermal exposures at 850°C, however, resulted in reduced crack growth resistance of the MMC. This was due to fiber degradation, fiber/matrix debonding, and an increase in matrix brittleness. Short-time isothermal exposures (up to about 10 h for Ti-6Al-4V/B_f, 30 h for Ti-6Al-4V/B_f (B_4C), and 60 h for Ti-6Al-4V/SiC_f(SCS-6)) improved the fatigue-

crack resistance. This was attributed to an energy-dissipating mechanism of fiber microcracking in the vicinity of the crack tip.

Cotterill and Bowen (1993) studied the fatigue crack growth behavior of SCS-6 fiber reinforced Ti-15V-3Al-3Sn-3Cr (Ti-15-3) composites. In general, the crack growth rates decreased with increasing crack length. This was attributed to crack tip "shielding" from the bridging fibers, which are stronger and stiffer than the matrix. When a single fiber fracture took place, however, the crack growth rate increased by two orders of magnitude. This was also accomplished by a single cycle overload, or by increasing the R-ratio (e.g., an increase in K_{min}). Cotterill and Bowen (1996) examined the effects of ΔK and K_{max}, the cyclic and static stress intensity components for fatigue crack growth, respectively. It was also shown that K_{max} controlled fiber fracture, but ΔK controlled the matrix crack growth rate. Thus, if fiber fracture takes place, K_{max} is the parameter that controls the crack growth rate. The crack growth rate was also shown to be dependent on ΔK. Below a critical value of ΔK, the crack arrested, but above that value, fiber fracture took place and the crack was able to propagate, Fig. 8.24. The transition from crack arrest to catastrophic failure is also affected by fiber strength distribution and specimen geometry (Liu and Bowen, 2002).

At very high temperatures in S-N fatigue, frequency plays a role in fatigue crack growth behavior. At lower frequencies, aging of the matrix and weakening of grain boundaries contribute to fracture in the composite (Cotterill and Bowen, 1993). Stress relaxation of the matrix during creep or due to hold times (or lower cyclic frequency) may also result in crack closure and aid in crack bridging (Zhang and Ghonem, 1995).

Rao et al. (1993) examined the fatigue crack growth behavior of $6061/SiC/40_f$ (SCS-8) composites in longitudinal and transverse orientations. Their results, shown in Fig. 8.25, indicate that the crack growth resistance of the composite was higher than that of the unreinforced alloy in the longitudinal orientation, but lower in the transverse orientation. Fiber debonding and crack deflection mechanisms toughened the composites in the L-T orientation, due to the relatively weak bonding between fiber and matrix provided by the C-rich coating on the SCS-8 fibers. These authors also proposed a mechanistic model for fatigue crack growth in the transverse orientation, whereby fiber debonds grew until a critical point where individual debonds were linked, resulting in fracture, Fig. 8.26. These authors also attempted to quantify the extent of bridging by the *ductile phase*, during transverse loading. The contribution from bridging, ΔK_b, was given by:

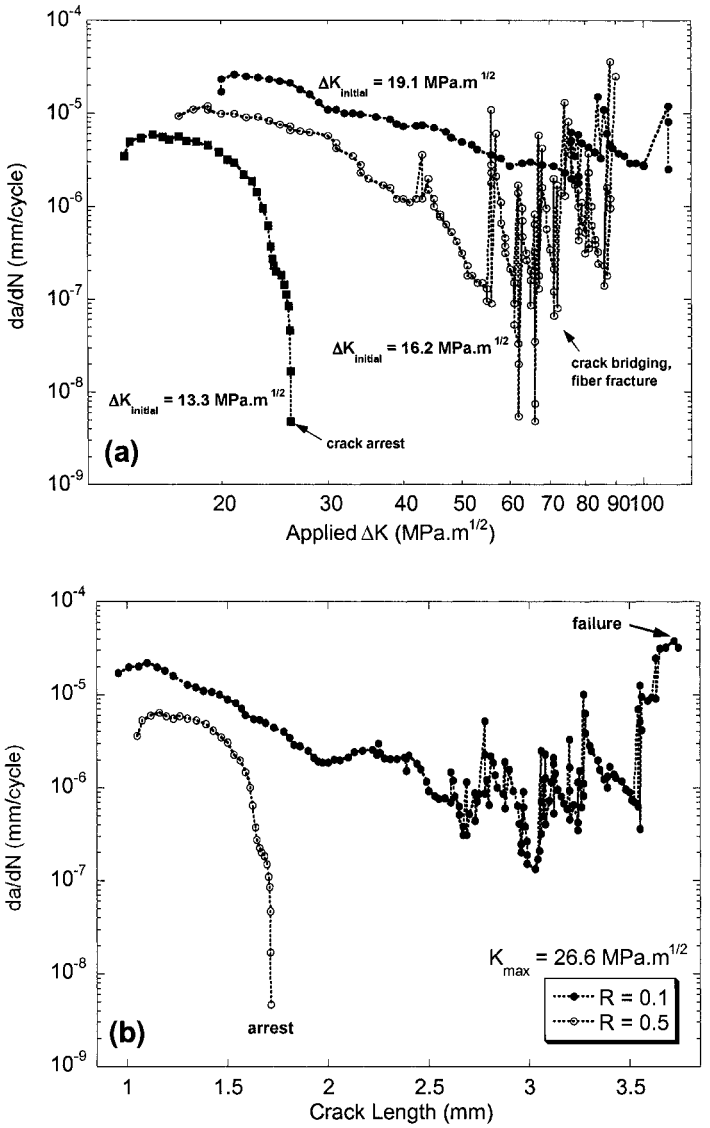

Fig. 8.24 Fatigue crack growth behavior of a SiC fiber reinforced Ti alloy composite: (a) influence of increasing ΔK and (b) influence of R-ratio. Critical values of K_{max} and ΔK are required to propagate the crack (after Cotterill and Bowen, 1996).

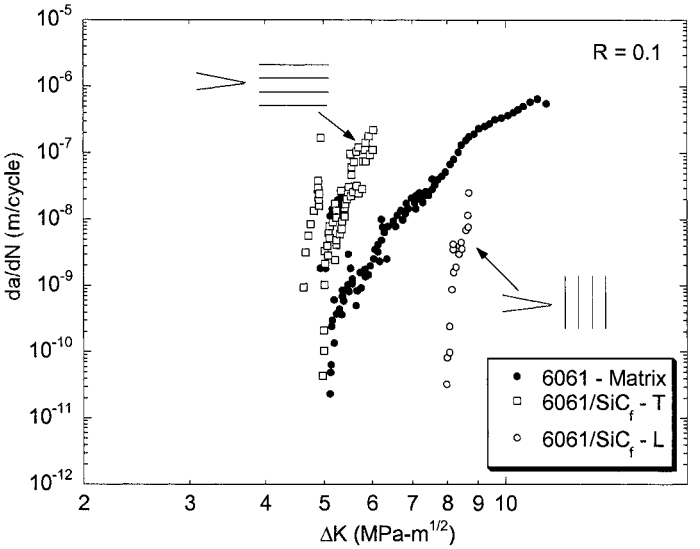

Fig. 8.25 Fatigue crack growth response of a SiC fiber reinforced Al 6061 matrix composite. The fatigue threshold in the longitudinal orientation is superior to that in the transverse orientation and that of the unreinforced alloy (after Rao et al., 1993).

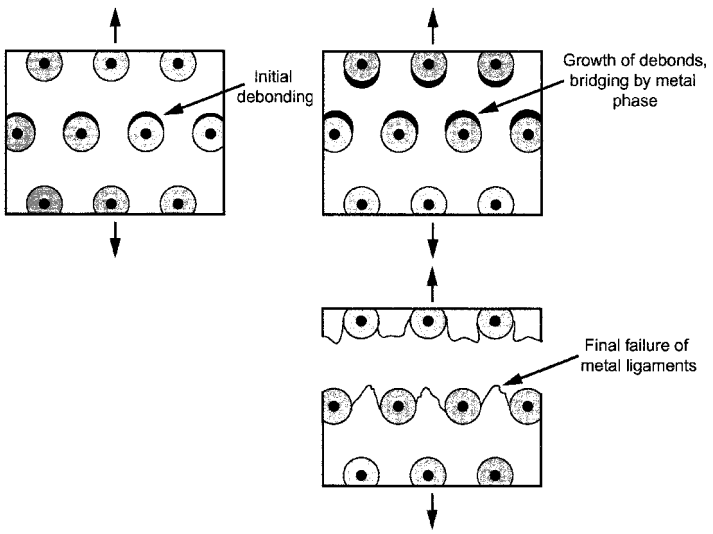

Fig. 8.26 Schematic of mechanisms for fatigue crack growth under transverse loading. Fiber debonds grow until a critical point where individual debonds are linked, resulting in fracture (after Rao et al., 1993).

$$\Delta K_b = \frac{2}{\sqrt{\pi a}} \int_0^{\ell} \sigma(x) F\left(\frac{x}{a}, \frac{a}{W}\right) dx$$

where a is the crack length, ℓ is the bridging zone length, W is the specimen width, $\sigma(x)$ is the stress distribution over the bridging zone, and x is the distance behind the crack tip. The total toughness, then, is given as:

$$K = K_o + \Delta K_b$$

where K_o is the intrinsic toughness of the composite. Assuming that $\sigma(x) = f\sigma_o$, where f is the fraction of ductile phase, and σ_o is the flow stress of the matrix,

$$\Delta K_b = 2f\sigma_o \sqrt{\frac{2\ell}{\pi}}$$

Using this relation the steady-state toughness of the composite was predicted to be around 12.4 $MPa\sqrt{m}$, which was slightly lower than that measured experimentally. The authors attributed the difference to an additional contribution from thermally-induced dislocation punching at the interface, which strengthened the matrix, as well as residual strains from plasticity.

Davidson et al. (1989) examined the fatigue crack growth behavior of an Al_2O_3 fiber reinforced Mg alloy composite (made by liquid infiltration). A simple model was developed to predict the crack growth rate as a function of ΔK. The cyclic crack opening displacement (COD), δ_c, is given by:

$$\delta_c = \frac{c_o \Delta K^2}{E_i}$$

where E_i is the elastic modulus of the matrix (E_m) or the composite (E_c). If the crack growth rate is assumed to be proportional to COD, then the Paris law can be written as:

$$\frac{da}{dN} = C\left[\left(\frac{E_m}{E_c}\right)^{\frac{1}{2}} \Delta K\right]^n$$

By incorporating shielding from the fibers, a lower bound was obtained, while an upper bound was obtained by incorporating the interaction between

the main crack and microcracks. By normalizing the crack growth data with respect to the modulus of the composite, good agreement was obtained for composites with varying fiber orientation, with respect to the loading axis, as well as with the unreinforced Mg alloy, Fig. 8.27.

Fatigue-crack propagation studies have also been conducted on aligned eutectic or *in situ* composites. Since many of these in situ composites are meant for high-temperature applications in turbines, their fatigue behavior has been studied at temperatures ranging from room temperature to 1100°C. The general consensus is that the mechanical behavior of *in situ* composites, i.e., static and cyclic strengths, is superior to that of the conventional cast superalloys (Stoloff, 1978).

8.2.2 Particle Reinforced MMCs

The crack growth behavior in particle reinforced MMCs is also very much dependent on reinforcement characteristics (Shang et al., 1988; Lukasak and Bucci, 1992; Allison and Jones, 1993; LLorca et al., 1994; Vasudevan and Sadananda, 1995), and on matrix microstructure (Bonnen et al., 1990; Sugimura and Suresh, 1992). In general, higher threshold values, ΔK_{th}, are observed for composites than for monolithic materials, Fig. 8.28. In addition,

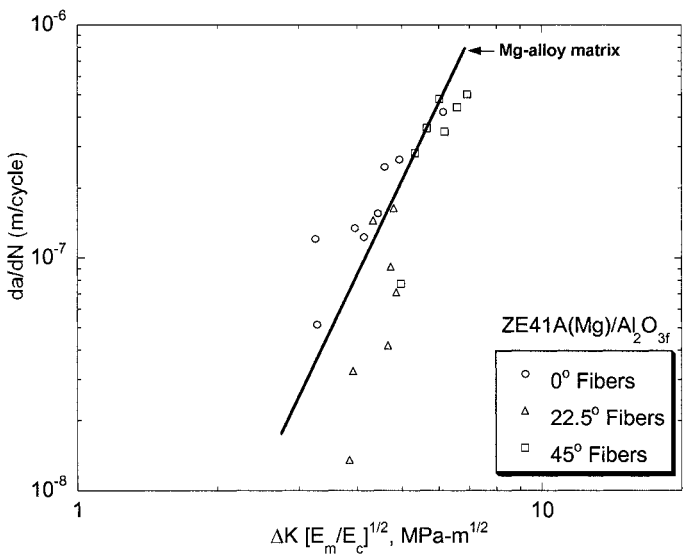

Fig. 8.27 Fatigue crack growth behavior of Mg(ZE41A)/$Al_2O_{3,f}$ composite, normalized by the Young's moduli of matrix and composite. Good agreement was obtained for composites with varying fiber orientation, as well as with the unreinforced Mg alloy (after Davidson et al., 1989).

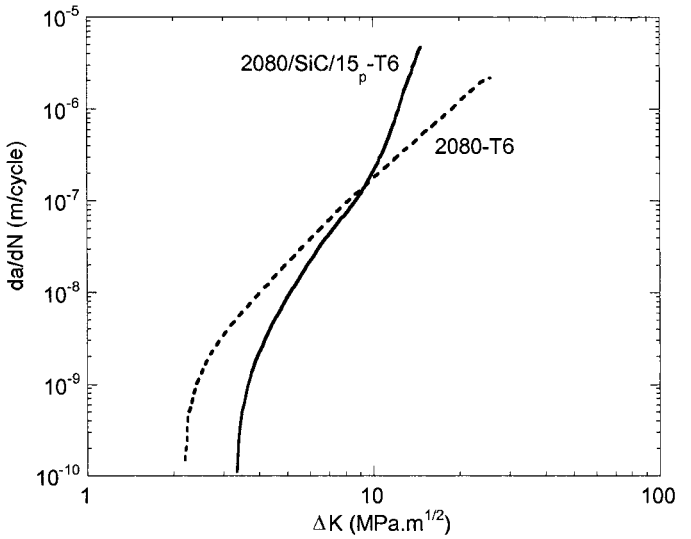

Fig. 8.28 Fatigue crack growth behavior of 2080-T6 alloy versus 2080/SiC/15_p-T6 composite. The composite exhibits a higher fatigue threshold and slightly higher Paris law slope (after Lukasak and Bucci, 1992).

increasing volume fraction of particles results in an increase in ΔK_{th}, Fig. 8.29. This can be attributed to the higher modulus of the composite, which results in a lower crack opening displacement for a given applied stress intensity factory. The Paris-law slope of da/dN vs ΔK curve for the composites is generally comparable to that of unreinforced alloys, although at very high ΔK, the crack propagation in the composites is much higher. This is due to lower fracture toughness of the composite, relative to the unreinforced alloy.

It is very important to note, however, that these trends are only true for composites with a constant matrix microstructure. Sugimura and Suresh, (1992), for example, examined the effect of SiC volume fraction on fatigue crack growth of cast MMCs. Because of the casting process, the grain size in the matrix was inversely dependent on the volume fraction of particles (see Chapter 4), i.e., the matrix microstructure changed with increasing volume fraction. This was because a higher volume fraction of particles resulted in a larger number of possible grain nucleation sites, and a finer overall grain size in the matrix of the composite. Thus, in their study, an increase in volume fraction of particles (i.e., a decrease in matrix grain size) contributed to a decrease in fatigue crack growth resistance, Fig. 8.30.

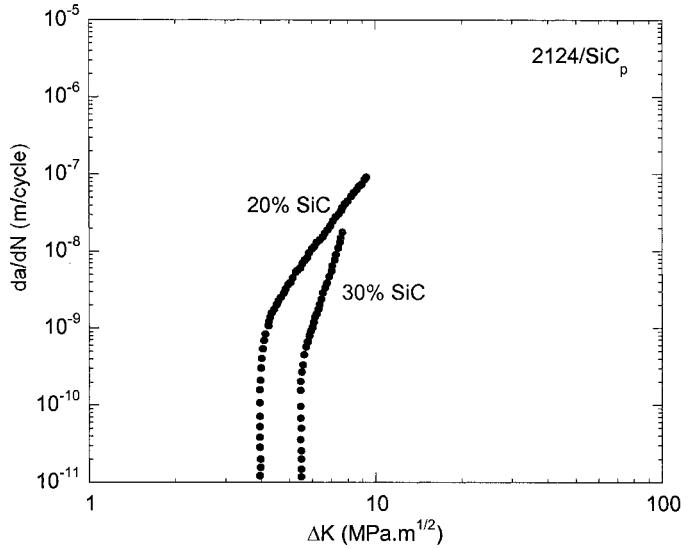

Fig. 8.29 Effect of volume fraction on fatigue crack growth of 2124/SiC$_p$ composites (after Bonnen et al., 1990). Increasing volume fraction results in an increase in fatigue threshold (the matrix microstructure of this powder metallurgy-processed composite was relatively constant).

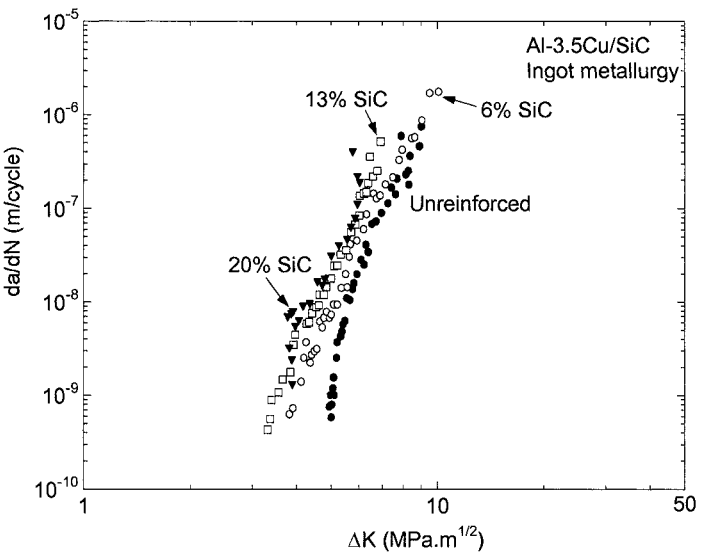

Fig. 8.30 Decrease in fatigue crack growth resistance with increasing volume fraction of SiC particles (cast composite). Because of the casting processing route, the matrix grain size at higher volume particle fractions decreased significantly, yielding lower fatigue resistance (after Sugimura and Suresh, 1992).

It is interesting to note that coarser particles provide better fatigue crack growth resistance, than finer particles, because of a large extent of roughness-induced crack closure (Shang et al., 1988), Fig. 8.31. Furthermore, experiments on overaged and underaged composites, showed little difference in fatigue crack growth resistance (Bonnen et al., 1990), indicating that the controlling deformation mechanisms are related to the particle characteristics and spatial distribution, Fig. 8.32. The fatigue crack growth behavior is also very much affected by the load ratio R ($K_{min}/K_{max} = \sigma_{min}/\sigma_{max}$). Figure 8.33(a) shows the fatigue crack growth behavior for a $2080/SiC/20_p$ composite at various R-ratios, ranging from −2 to 0.8. With increasing R-ratio, the fatigue threshold decreases and the Paris law slope increases. These data can be further represented by using the two-parameter approach of ΔK versus K_{max}, by Vasudevan et al. (1994), shown in Fig. 8.33(b). This approach can be understood simply by the fact that critical values of both ΔK and K_{max} must be met for the crack to propagate. Thus, with increasing crack growth rate, at higher R-ratios, for a given value of ΔK a much smaller value of K_{max} needs to be applied for the crack to propagate.

The effects of ΔK and K_{max} can be explained in terms of the plastic zone size at the crack tip, and reinforcement/crack interactions (Shang et al., 1988; Chawla and Chawla, 2004). Figure 8.34 shows a schematic of the observed behavior during fatigue crack growth (Chawla and Chawla, 2004). At low K_{max} and/or ΔK the fatigue crack propagates around the particles, while at high K_{max} and/or ΔK particle fracture takes place ahead of the crack tip, resulting in relatively planar crack growth. This behavior is can be explained by the size of the plastic zone, relative to the size and fracture strength of the particles. At low K_{max} and/or ΔK, the plastic zone at the crack tip is on the order of the particle size. Thus, crack growth takes place around the SiC particles, Fig. 8.35, and crack arrest and crack deflection mechanisms contribute to enhanced resistance to crack growth. Ayyar et al. (2005) modeled the crack growth behavior in an SiC particle reinforced composite, by using the two-dimensional microstructure of the material as a basis for the finite element model. A modified crack closure criterion was used to calculate the stress intensity at the crack tip, while the maximum circumferential tensile stress criterion was used to determine the direction of crack propagation. The predicted response qualitatively shows the same behavior as that observed in the experiment, i.e., the cracks grow around the SiC particles in a somewhat tortuous fashion, Fig. 8.36. Similar models have been developed by Boselli et al. (2001), for perfectly circular particles of single size.

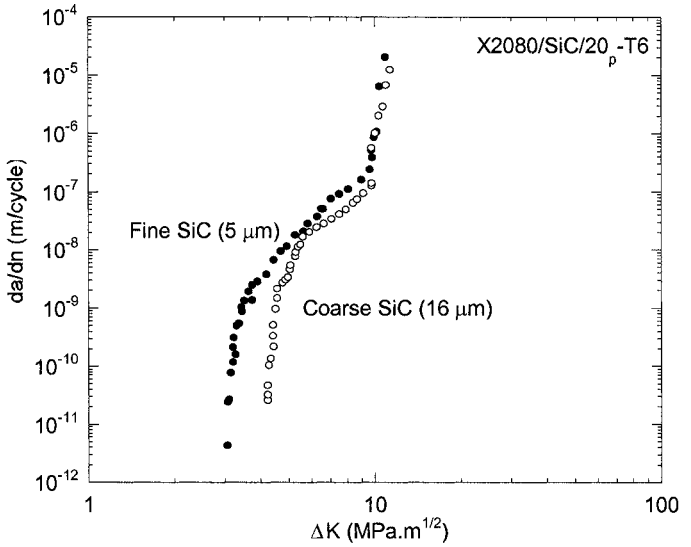

Fig. 8.31 Effect of particle size on fatigue crack growth behavior in a 2080/SiC/20p-T6 composite. The larger particles results in a larger degree of roughness-induced closure, thus increasing the fatigue threshold (after Shang et al., 1998).

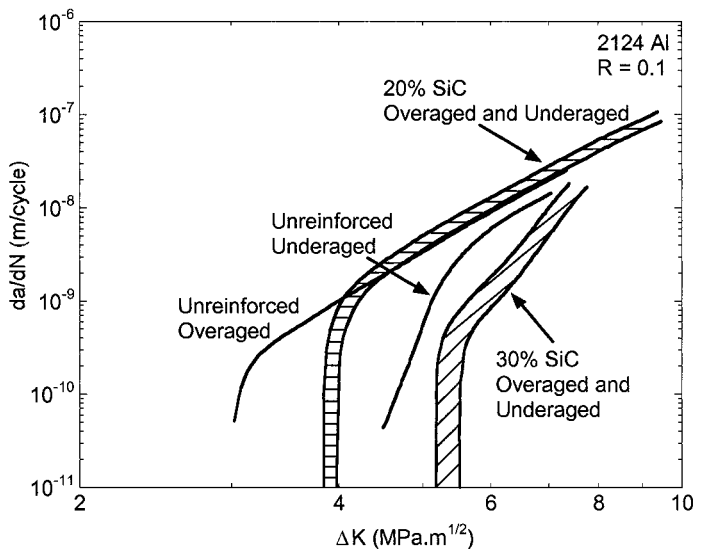

Fig. 8.32 Fatigue crack behavior for 2124 alloy and its composites in underaged and overaged conditions. While the unreinforced alloy is sensitive to aging, the composites are not, indicating that the particles control fatigue crack growth behavior (after Bonnen et al., 1990).

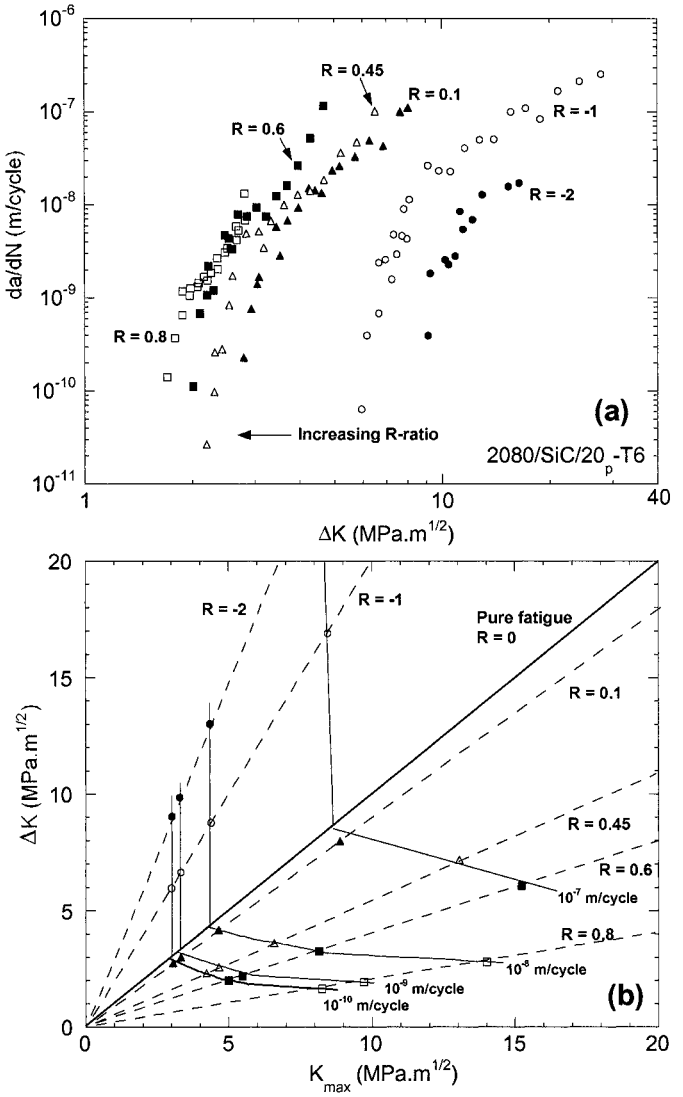

Fig. 8.33 Effect of R-ratio on fatigue crack growth of 2080/SiC/20$_p$: (a) da/dN vs. ΔK behavior, showing decreasing fatigue threshold and increasing Paris law slope with increasing R; and (b) same data plotted using ΔK vs. K_{max} approach, showing decreasing resistance to fatigue crack growth with increasing K_{max} (after Ganesh and Chawla, 2004).

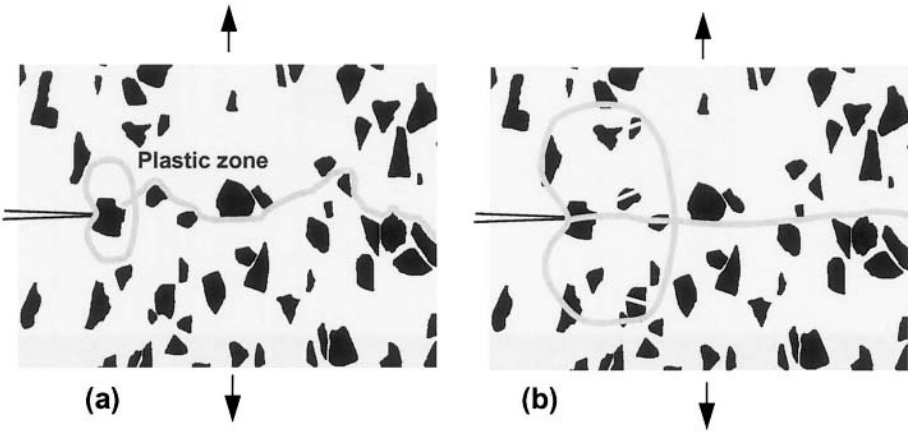

Fig. 8.34 Schematic of fatigue damage in particle reinforced MMCs: (a) low R-ratio, plastic zone is on the order of the particle size, and crack growth is tortuous, and (b) high R-ratio, plastic zone is much larger than the particle size resulting in particle fracture ahead of the crack tip, and planar crack growth (after Chawla and Chawla, 2004).

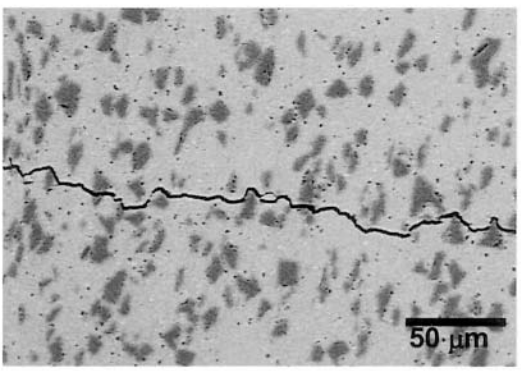

Fig. 8.35 Fatigue crack growth behavior of 2080/SiC/20_p; the crack propagates around the SiC particles.

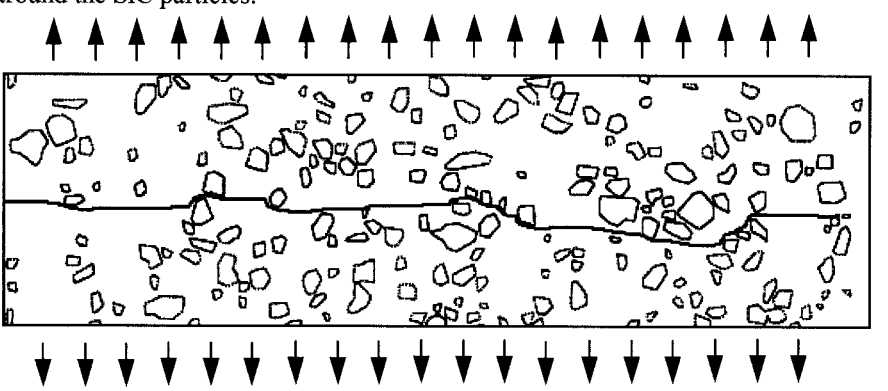

Fig. 8.36 Microstructure-based finite element model prediction of crack growth in an SiC particle reinforced Al matrix composite, showing tortuous crack growth around the reinforcement particles (after Ayyar et al., 2005).

At high K_{max} and/or ΔK, the plastic zone is large enough to engulf several particles, so particle fracture ahead of the crack tip takes place, and the crack growth is relatively linear. This behavior is confirmed by the degree of experimentally measured particle fracture at R-ratios of 0.1 and 0.8, respectively, Fig. 8.37. Note that the degree of particle fracture is much higher at the higher R-ratio, i.e., it is driven by K_{max}.

We end this section by discussing the fatigue damage mechanisms in compression-compression fatigue. Here, the nature of damage is quite different from that observed in tension-tension fatigue. Fig. 8.38 shows the fracture surface of a 2080/SiC/20_p composite after fatigue growth for an R-ratio of −2. Observe the wear markings on the SiC particle surface, and that spherical particles are present on the surface. Energy-dispersive spectroscopy (EDS) analysis showed these particles to be Al_2O_3, indicating that matrix particles likely oxidized were wedged into the SiC particle. A similar behavior has been observed in steels containing carbide particles (Aswath et al., 1988).

8.2.3 Hybrid and Laminated Composites

Composites containing more than one type of reinforcement are called hybrid composites. Such composites, by using two or more type of reinforcements, extend the idea of tailor-making a composite material to

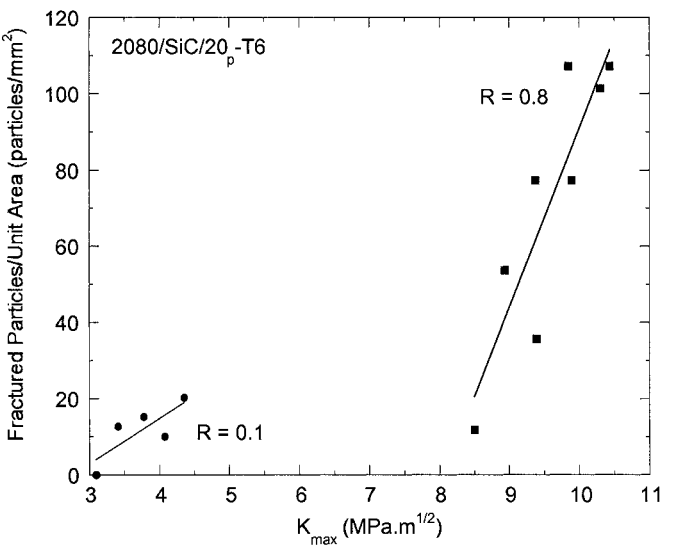

Fig. 8.37 Degree of particle fracture in 2080/SiC/20_p versus applied K_{max}, at R-ratios of 0.1 and 0.8. Higher K_{max} results in a significantly larger degree of particle fracture.

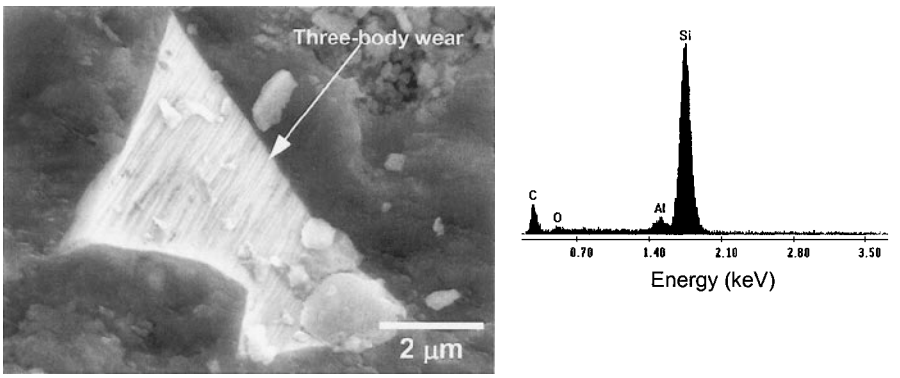

Fig. 8.38 Fatigue fracture surface after compression fatigue (R = −2). Debris from the fatigue process (Al_2O_3, from EDS spectra on the right) is embedded into the SiC particles resulting in three-body wear.

meet specific property requirements. Partial replacement of expensive fibers by cheaper but adequate fiber types is another attractive feature of hybrid composites.

Metallic sheet laminated composites have been shown to have improved fatigue resistance over their monolithic counterparts (Chawla and Liaw, 1979). There are two possible crack geometries: Crack arrester and crack divider geometries. In the crack arrest geometry, with the crack growing perpendicular to the thickness of the composite, the mechanism proposed by Cook and Gordon (1964) would appear to work (see also chapter 5). According to this model, if the interface is weak, then the crack bifurcates and changes its direction when it reaches the interface, and thus the failure of the composite is delayed. The improved fatigue crack propagation resistance in crack divider geometry has been verified by a number of researchers (McCartney et al., 1967, Taylor and Ryder, 1976, and Pfeiffer and Alic, 1978). This improved performance has been attributed either to interfacial separation, which removes the triaxial state of stress, or to a holding back of crack at the interface in the faster crack-propagating component by the slower crack-propagating component.

An interesting type of hybrid composite consists of alternating layers of high-strength aluminum alloy sheets and layers of unidirectional aramid or glass fibers in an epoxy matrix. There are two types of such laminates: ARamid ALuminum Laminate (ARALL) and GLAss REinforced (GLARE) laminate. Improved fatigue resistance of ARALL or GLARE over that of monolithic aluminum structures is the main attractive feature. Cracks in aluminum can grow only a short distance before being blocked by the aramid or glass fibers spanning the crack tip, Fig. 8.39 (Wu and Yang,

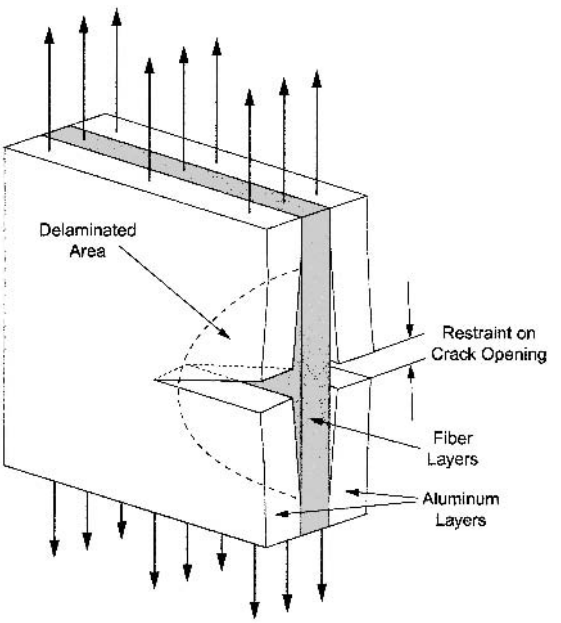

Fig. 8.39 Schematic of fatigue damage in ARALL or GLARE. Cracks can grow only a short distance before being blocked by the aramid or glass fibers spanning the crack tip (after Wu and Yang, 2005).

2005). Figure 8.40 shows the slow fatigue-crack growth characteristics of ARALLs compared with two monolithic aluminum alloys (Mueller and Gregory, 1988). ARALL has been used in tension-dominated fatigue structures such as aircraft fuselage, lower-wing, and tail skins. The use of ARALL resulted in 15-30% weight savings over conventional construction. GLARE has been chosen for use in the fuselage of the twin-deck, 550-seat, Airbus 380 aircraft. Besides having superior fatigue behavior, Glare is also lighter than aluminum, cutting the weight of the Airbus A380 by 1,000 kg. Another version of hybrid laminated MMCs is a family of layered composites consisting of metallic outer skins with a viscoelastic core material (for example, polyethylene, nylon, polypropylene, paper, or cork). Such composites are useful where sound and vibration dampening are required. The viscoelastic layer provides a high loss factor, i.e., a high capacity to convert vibrational energy to heat.

Other innovative approaches to engineering hybrid composites include laminated composites of SiC particle reinforced Al layers diffusion bonded to pure Al alloy layers, Fig. 8.41(a) (Hassan et al., 2004). It was shown that incorporation of the ductile metallic layers resulted in lower crack growth rate in the Paris law regime, higher fracture toughness, and slightly lower fatigue crack threshold, compared to conventional particle reinforced

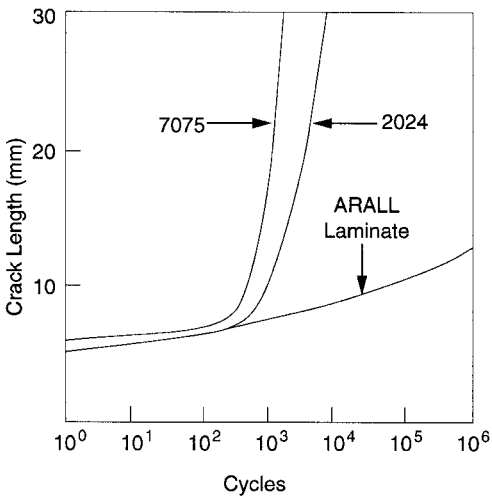

Fig. 8.40 Fatigue crack growth behavior of ARamid ALuminum Laminate (ARALL) compared to conventional 7075 and 2024 aluminum alloys (after Mueller and Gregory, 1988). The ARALL has significantly better crack growth resistance.

MMCs, Fig. 8.41(b). The authors attributed the resistance to crack growth to the higher Young's modulus of the laminate, which resulted in a lower crack opening displacement, for a given applied stress intensity factor. The elastic mismatch also resulted in a crack tip shielding effect at the interface between the layers.

8.3 THERMAL FATIGUE

The problem of thermal expansion mismatch between the components of a composite is a very general and serious one (Chawla, 1997). Thermal stresses arise in composite materials because of the large differences in the thermal expansion coefficients (α) of the fiber and the matrix. It should be emphasized that thermal stresses in composites will arise even if the temperature change is uniform throughout the volume of the composite. Such thermal stresses can be introduced in composites during cooling from high fabrication, annealing, or during any temperature excursions (inadvertent or by design) during service. Turbine blades, for example, are very much susceptible to thermal fatigue.

We described the origin and analysis of thermal stresses in chapter 6. To recapitulate, the magnitude of thermal stresses in composites is proportional to the thermal strain, $\Delta\alpha\Delta T$, where $\Delta\alpha$ is the difference in the expansion coefficients of the two components, and ΔT is the amplitude of the thermal cycle. In MMCs, the matrix generally has a much higher coefficient of

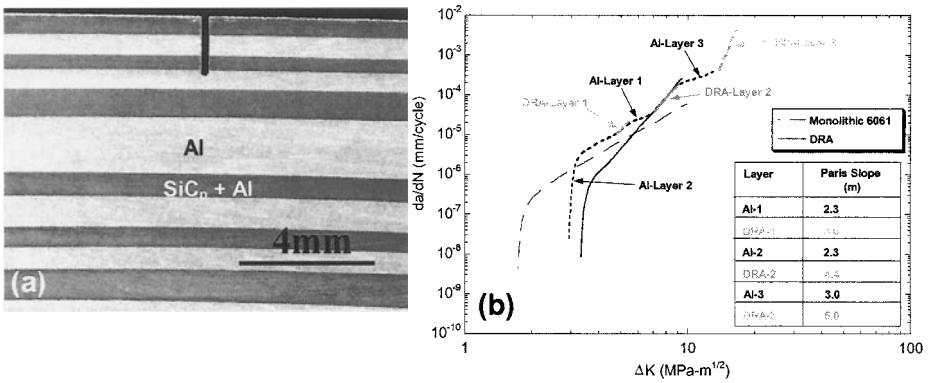

Fig. 8.41 (a) Notched hybrid composite of pure Al and SiC particle reinforced Al composite (courtesy of J. Lewandowski), and (b) fatigue crack growth behavior, showing enhanced crack growth resistance in the Paris law regime (after Hassan et al., 2004).

thermal expansion than the reinforcement. Rather large internal stresses can result when fiber reinforced composites are heated or cooled through a temperature range. When this happens in a repeated manner, we have *thermal fatigue,* because the cyclic stress is thermal in origin. Thermal fatigue can cause plastic deformation in a ductile metallic matrix (Chawla, 1973a; Chawla 1973b). Cavitation in the matrix and fiber/matrix debonding are the other forms of damage observed due to thermal fatigue in composites (Kwei and Chawla, 1992; Xu et al., 1995). Figure 8.42 shows a scanning electron micrograph of an alumina fiber reinforced magnesium alloy matrix that was subjected to different thermal cycles between room temperature and 300°C.

Xu et al. (1995) examined the thermal cycling behavior of a ZE41A Mg alloy reinforced with 35% Al_2O_3 fibers. They quantified the damage during thermal cycling by measuring the change in Young's modulus and density as a function of thermal cycles. The damage during thermal cycle may also be quantified by a change in damping behavior of the composite (Carreno-Morelli et al., 2001). A damage parameter was defined, where the damage in Young's modulus, for example, is given by:

$$D_E = 1 - \left(\frac{E_n}{E_o}\right)$$

where E_n is the Young's modulus after n cycles, and E_o is the initial Young's modulus prior to cycling. A similar approach was used to monitor damage in density, ρ. In order to correlate D_E and D_ρ, Mackenzie's equation was invoked (Mackenzie, 1950):

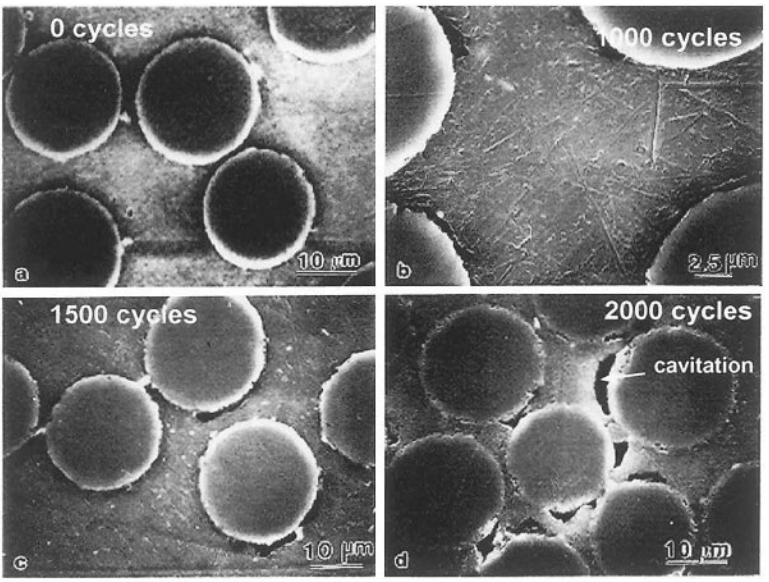

Fig. 8.42 Evolution of thermal fatigue damage in an Mg/Al_2O_{3f} composite. With increasing cycles interfacial cavitation takes place due to internal stress mismatch between fiber and matrix (after Xu et al., 1995).

$$E_n = E_o\left(1 - aV_v - bV_v^2\right)$$

where V_v is the volume fraction of voids, and *a* and *b* are constants of a fully dense material. For materials with Poisson's ratio of 0.3, a = 1.91 and b = −0.91. By incorporating these equations and using the rule of mixtures for the density of the composite, $\rho_c = \rho_f V_f + \rho_m V_m$, the following relation is obtained:

$$D_E = b\left(\frac{\rho_o}{\rho_m}\right)D_n + b_1\left[\left(\frac{\rho_o}{\rho_m}\right)D_\rho\right]^2$$

where ρ_m is the density of the matrix. Figure 8.43 shows a plot of experimental and predicted values of D_E versus D_ρ, showing very good agreement. In general, one can reduce the damage in the matrix by choosing a matrix material that has a high yield strength and a large strain to failure (i.e., ductility). The eventual fiber/matrix debonding can only be avoided by choosing the components such that the difference in the thermal expansion characteristics of the fiber and the matrix is low.

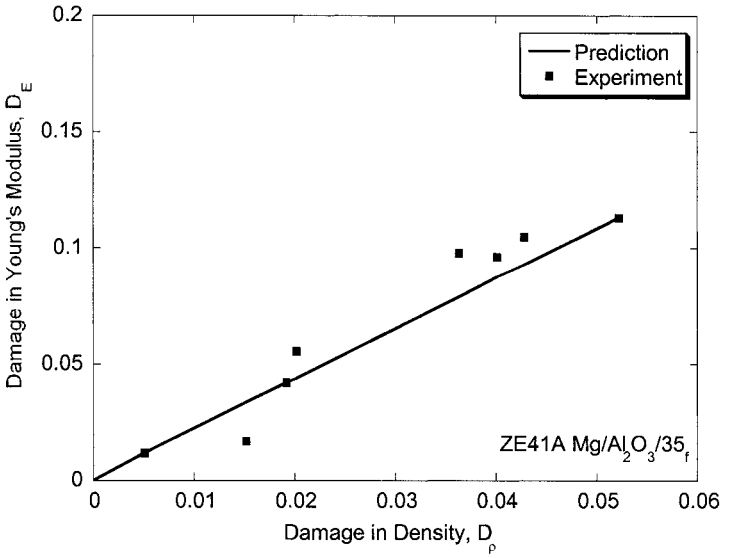

Fig. 8.43 Damage in Young's modulus versus damage in density for a $Mg/Al_2O_3/35_f$ composite showing good correlation between predicted and experimental results (Xu et al., 1995).

One type of thermal fatigue test involves cycling temperature of the sample while its gage length is kept constant. This constraint results in an internal stress on the sample. Thus, measurement of the internal stresses generated when subjecting a composite to thermal cycling can be used to evaluate study thermal fatigue. Figure 8.44 shows the results of cycling between 300°C and 500°C for alumina fiber/Al-Li composite (Kwei and Chawla, 1992). The alumina fibers were unidirectionally aligned parallel to the stress axis, and the fiber volume fraction was 35%. The plot shows the variation of the maximum stress in tension and compression as a function of number of cycles. The initial rise in the maximum tensile stress curve is due to the work hardening of the aluminum alloy matrix caused by the thermal stresses. With continued cycling, the microstructural damage sets in, and a plateau in the maximum tensile stress versus cycles curve is obtained as long as the strength increase due to work hardening of the matrix is balanced by the strength decrease due to microstructural damage, e.g., voiding at the interface. The maximum compressive stress, however, decreases with cycling to a plateau value. This may be due to the Bauschinger effect, i.e., a higher strength in tension results in a concomitant lowering of the strength in compression. Eventually, the alumina fibers suffer fracture, which causes the tensile stress curve in Fig. 8.44 to decrease.

Superimposed effects of mechanical and thermal loading are important in a variety of applications such as in an automotive engine or gas turbine. Two

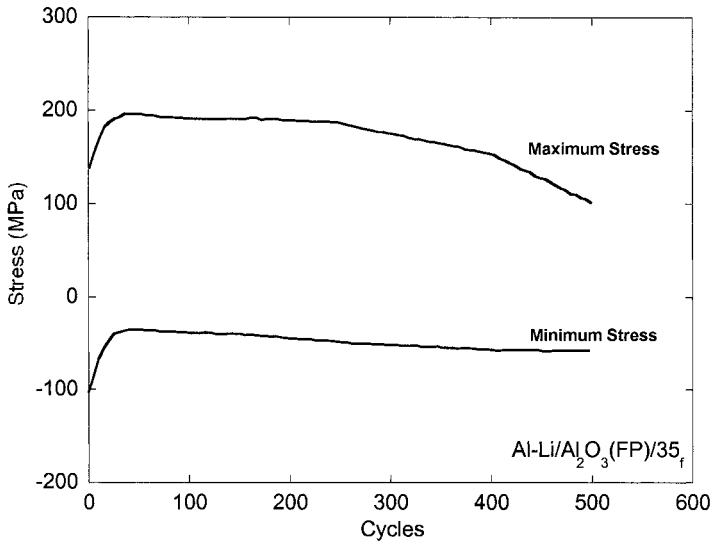

Fig. 8.44 Evolution of stess during strain-controlled thermal cycling of Al-Li/Al_2O_3/35_f composite (after Kwei and Chawla, 1992). With increasing thermal cycles, relaxation processes such as interfacial cavitation result in stress relaxation.

types of thermomechanical loading may be applied: (a) in-phase loading, where the maximum and minimum stress take place at maximum and minimum temperature, respectively; and (b) out-of-phase loading, where the maximum stress and minimum stress are opposite to the maxima and minima in temperature. The nature of thermomechanical loading has a direct influence on the internal stress in the fiber and matrix. Consider the case of out-of-phase loading. During cooling, the ceramic fiber is in a state of residual compression, and the metal matrix is in tension. Thus, at the minimum temperature, where the applied stress is a maximum, the total stress on the matrix will be enhanced, while that in the fiber will be lower. In in-phase loading, at the maximum temperature, the fiber is in tension while the matrix is in compression. Since the maximum temperature corresponds to the point of maximum stress, the stress on the fiber is maximized.

The effects of the internal stress during out-of-phase and in-phase TMF for a Ti-6242/SiC_f composite are shown in Fig. 8.45(a) (Bettge et al., 2003; Peters et al., 2004). In general, the fatigue life under TMF loading is significantly lower than in pure mechanical low cycle fatigue. In-phase loading results in lower overall fatigue resistance, while out-of-phase loading exhibits an abrupt decrease in fatigue life at about 10^3 cycles. Due to the different internal stress states, the mechanisms for fracture in TMF are also quite different. Under in-phase loading, matrix relaxation takes place which results in a gradual increase in the stress in the fiber. Thus, fatigue life is creep-

controlled, Fig. 8.45. In out-of-phase loading, the strain range in the matrix is very large, so the damage is primarily matrix-controlled. With matrix crack, oxygen ingression takes place, and when the cracks reach the fiber/matrix interface, oxidation and fracture of the fiber take place, Fig. 8.45(b). Thus, at higher stress the fracture is fiber-controlled, with decreasing stress multiple matrix cracks and fiber bridging were observed. Thermal cycling damage in discontinuously reinforced MMCs is somewhat lower than that of continuous fiber reinforced MMCs, because diffusional relaxation of the matrix is easier (the constraint on the matrix is lower for

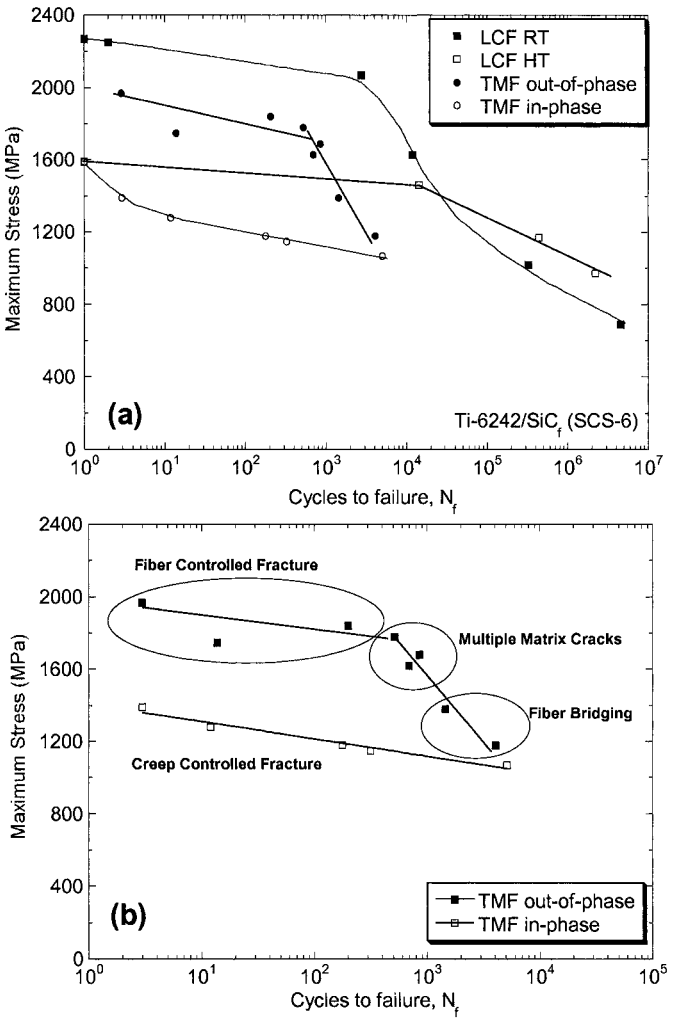

Fig. 8.45 Comparison of thermomechanical fatigue and low cycle fatigue of a Ti/SiC$_f$ composite: (a) stress versus cycles behavior, showing the more damaging effect of thermal fatigue, and (b) damage mechanisms (after Bettge et al., 2003).

discontinuous reinforcement). Very large plastic strains (on the order of 150% for Al composites with 20 and 30% SiC) have been observed during thermal cycling (Pickard and Derby, 1990). In addition, a significant increase in surface roughness of the composite has been observed, by Rezai-Aria et al. (2003). They studied the thermal cycling behavior of an $Al/Al_2O_3/15_{sf}$ (Saffil) composite. The increase in surface roughness was attributed to the higher mobility of dislocations near the free surface. Within the bulk of the material, a cellular dislocation structure evolved during thermal cycling.

References

Allison, J.E., and J.W. Jones, (1993) in *Fundamentals of Metal Matrix Composites*, S. Suresh, A. Mortensen, and A. Needleman, eds., Butterworth-Heinemann, Stoneham, MA, p. 269.

Almond, E.A., and B. Roebuck, (1980) *Metals Technology*, **7**, 83-85.

Arsenault, R.J., and U.T.S. Pillai, (1996) *Metall. Mater. Trans.*, **27A,** 995-1001.

Arsenault, R.J., and S.B. Wu, (1987) *Mater. Sci. Eng.*, **96,** 77-88.

Aswath, P.B, S. Suresh, D.K. Holm, and A.F. Blom, (1988) *J. Eng. Mater. Tech.*, **110** 278-85.

Ayyar, A., J.J. Williams, and N. Chawla, (2005) *Comp. Sci. Tech.*, submitted.

Baker, A.A., D.M. Braddick, and P.W. Jackson, (1972) *J. Mater. Sci.*, **7**, 747-762.

Bauschinger, J., (1886) *Mitt: Mech-Tech Lab.*, XIII Munchen.

Bettge, D., B. Gunther, W. Wedell, P.D. Portella, J. Hemptenmacher, and P.W.M. Peters, (2004) in *Low Cycle Fatigue 5*, (P. D. Portella, H. Sehitoglu, K. Hatanaka, eds.), DVM, Berline, pp. 81-86.

Blatt, D., J.R. Jira, and J.M. Larsen, (1995) *Scripta Metall. Mater.*, **33**, 939-944.

Bonnen, J.J., C.P. You, J.E. Allison, and J.W. Jones, (1990) in *Proceedings of the International Conference on Fatigue,* Pergamon Press, New York, pp. 887–892.

Boselli, J., P.D. Pitcher, P.J. Gregson, and I. Sinclair, (2001) *Mater. Sci. Eng.*, **A300**, 113-124.

Calabrese, C., and C. Laird, (1974a) *Mater. Sci. Eng.,* **13**, 141 - 157.

Calabrese, C., and C. Laird, (1974b) *Mater. Sci. Eng.,* **13**, 159 - 174.

Carreno-Morelli, E., N. Chawla, and R. Schaller, (2001) *J. Mater. Sci. Lett.*, **20**, 163-165.

Champion, A.R., W.H. Krueger, H.S. Hartman, and A.K. Dhingra, (1978), in *Proc. 1978 Intl. Conf. Composite Materials* (ICCM/2), TMS-AIME, New York, p. 883.

Chawla, K.K, (1973a) *Metallography*, **6**, 155.

Chawla, K.K., (1973b) *Phil. Mag.*, **28**, 401.

Chawla, K.K., (1998) *Composite Materials: Science & Engineering*, Springer-Verlag, New York.

Chawla, K.K., (1975) *Fiber Sci. Tech.*, **8**, 49.

Chawla, K.K., (1991) in *Metal Matrix Composites: Mechanisms and Properties*, R.K. Everett and R.J. Arsenault, eds., Academic press, pp. 235-253.

Chawla, K.K., and N. Chawla, (2004) in *Kirk-Othmer Encyclopedia*, John-Wiley and Sons, New York.

Chawla, K.K., and P.K. Liaw, (1979) *J. Mater. Sci.*, **14,** 2143.

Chawla, K.K., and M. Metzger, (1972) *J. Mater. Sci.*, **7**, 34.

Chawla, N., (1997) *Metall. Mater. Trans.*, **28A**, 2423.

Chawla, N., and J.E. Allison, (2001) in *Encyclopedia of Materials: Science and Technology*, vol. 3, (B. Ilschner and P. Lukas, eds.), Elsevier Science, pp. 2969-2974.

Chawla, N., C. Andres, J.W. Jones, and J.E. Allison, (1998a) *Metall. Mater. Trans.*, **29A**, 2843.

Chawla, N., C. Andres, J.W. Jones, and J.E. Allison, (1998b) *Scripta Mater.*, **38**, 1596.

Chawla, N., L.C. Davis, C. Andres, J.E. Allison, J.W. Jones, (2000a) *Metall. Mater. Trans.*, **31A**, 951-957.

Chawla, N., U. Habel, Y.-L. Shen, C. Andres, J.W. Jones, and J.E. Allison, (2000b) *Metall. Mater. Trans.*, **31A**, 531-540.

Chawla, N., J.W. Holmes, and R.A. Lowden, (1996) *Scripta Mater.*, **35**, 1411.

Chawla, N., J.W. Jones, and J.E. Allison, (1999).in *Fatigue '99* (X.R. Wu and Z.G. Wang, eds.), EMAS/HEP.

Chawla, N., M. Kerr, and K.K. Chawla, (2005) *J. Am. Ceram. Soc.*, **88**, 101-108.

Chawla, N., and Y.-L. Shen, (2001) *Adv. Eng. Mater.*, **3**, 357-370.

Cook, J., and J.E. Gordon, (1964) *Proc. Roy. Soc. Lond.*, **A282**, 508.

Cotterill, P.J., and P. Bowen, (1993) *Composites*, **24**, 214-221.

Cotterill, P.J., and P. Bowen, (1996) *Mater. Sci. Tech.*, **12,** 523-529.

Couper, M.J., and K. Xia, (1991) in *Metal Matrix Composites - Processing, Microstructure and Properties*, (N. Hansen et al., eds.), Riso National Laboratory, Roskilde, Denmark, p. 291.

Davidson, D.L., K.S. Chan, A. McMinn, and G.R. Leverant, (1989) *Metall. Trans.*, **20A**, 2369-2378.

Doker, H., and G. Marci, (1983) *Int. J. Fatigue*, **5**, 187-191.
Foulk III, J.W., D.H. Allen, and K.L.E. Helms, (1998) *Mech. Mater.*, **29**, 53-68.
Ganesh, V.V., and N. Chawla, (2004) *Metall. Mater. Trans.*, **35A**, 53-62.
Gomez, J.P., and F.E. Wawner, (1988) personal communication.
Gouda, M., K.M. Prewo, and A.J. McEvily, (1981) in *Fatigue of Fibrous Composite Materials*, p. 101, ASTM STP, 723, Amer. Soc. Testing and Materials, Philadelphia.
Hack, J.E., R.A. Page, and G.R. Leverant, (1987) *Metall. Trans.*, **15A**, 1389.
Hall, J., J.W. Jones, and A. Sachdev, (1994) *Mater. Sci. Eng.*, **A183**, 69.
Harmon, D.M., C.R. Saff, and C.T. Sun, (1987) AFW AL- TR-87-3060. Air Force Wright Aeronautical Labs., Dayton, Ohio.
Hassan, H.A., J.J. Lewandowski, and M.H. Abd El-latif, (2004) *Metall. Mater. Trans.*, **35A**, 45-52.
Johnson, W.S., (1982) in *Damage in Composite Materials, ASTM STP 775*, American Society for Testing and Materials, Philadelphia, p. 83.
Johnson, W.S., (1988) in *Mechanical and Physical Behavior of Metallic and Ceramic Composites*, 9th Risø Intl. Symp. on Metallurgy and Materials Science, Rise Nat. Lab., Roskilde, Denmark.
Johnson, W.S., and R.R. Wallis, (1986) in *Composite Materials: Fatigue and Fracture, ASTM STP 907*, American Society for Testing and Materials, Philadelphia, p. 161.
Kerr, M., N. Chawla, and K.K. Chawla, (2005) *JOM*, **2**, 67-70.
Kindermann, P., P. Schlund, H.-G. Sockel, M. Herr, W. Heinrich, K. Görtring, and U. Schleinkofer, (1999) *Int. J. Refractory & Hard Materials*, **17**, 55
Kwei, L.K, and K.K. Chawla, (1992) *J. Mater. Sci.*, **27**, 1101-1106.
Lewandowski, J.J., (2000) in *Comprehensive Composite Materials*, vol. 3, (A. Kelly and C. Zweben, eds.), Elsevier Press, pp. 151-187.
Li, C., and F. Ellyin, (1996) *Mater. Sci. Eng.*, **A214**, 115.
Liu, J., and P. Bowen, (2002) *Acta Mater.*, **50**, 4205-4218.
Liu, J., and P. Bowen, (2003) *Metall. Mater. Trans.*, **34A**, 1193-1202.
LLorca, J., (1994) *Acta Metall. Mater.*, **42**, 151-162.
LLorca, J., (2002) *Prog. Mater. Sci.*, **47**, 283-353.
LLorca, J., A. Needleman, and S. Suresh, (1990) *Scripta Metall. Mater.*, **24**, 1203.
LLorca, J., J. Ruiz, J.C. Healy, M. Elices, and C.J. Beevers, (1994) *Mater. Sci. Eng.*, **A185**, 1-15.
LLorca, J., S. Suresh, and A. Needleman, (1992) *Metall. Mater. Trans.*, **23A**, 919-933.
Lukasak, D.A., and R.J. Bucci, (1992) Alloy Technology Div. Rep. No. KF-34, Alcoa Technical Center, Alcoa, PA.

Lukasak, D.A., and D.A. Koss, (1993) *Composites*, **24**, 262.
Mackenzie, J.K., (1950) *Proc. Phys. Soc.*, **B63**, 2.
Mall, S., and B. Portner, (1992) *J. Eng. Mater., Tech.*, **114**, 409-415.
McCartney, R.F., R.C. Richard, and P.S. Trozzo, (1967) *Trans. ASM*, **60**, 384.
McGuire, M.A., and B. Harris, (1974) *J. Phys., Appl. Phys.*, **7**, 1788.
Majumdar, B.S., and G.M. Newaz, (1995) *Mater. Sci. Eng.*, **A200**, 114-129.
Meyers, M.A., and K.K. Chawla, (1999) *Mechanical Behavior of Materials*, Prentice-Hall.
Mott, N.F., (1952) *Phil.Mag.*, **43**, 1151.
Mueller, L.R., and M. Gregory, (1988) paper presented at First Annual Metals and Metals Processing Conf., SAMPE, Cherry Hill, NJ.
Orowan, E., (1959) in *Internal Stresses and Fatigue in Metals*, (G.M. Rassweiler and W.L. Grube, eds.), Elsevier Press, New York.
Page, R.A., J.E. Hack, R. Sherman, and G.R. Leverant, (1987) *Metall. Trans.*, **15A**, 1397.
Paris, P.C., M.P. Gomez, and W.P. Anderson, (1961) *The Trend in Engineering*, **13**, 9.
Paris, P.C., and F. Erdogan, (1963) *J. Basic. Eng. Trans. ASME*, **85**, 528.
Pfeiffer, N.J., and J.A. Alic., (1978) *J. Eng. Mater. Tech.*, **100**, 32.
Peters, P.W.M., J. Hemptenmacher, B. Gunther, D. Bettge, and P.D. Portella, (2004) in *Proc. ECCM-11*.
Pickard, S.M., and B. Derby, (1990) *Acta Metall. Mater.* **38**, 2537-2552.
Poza, P., and J. LLorca, (1999) *Metall. Mater. Trans.*, **30A**, 857.
Pugsley, V.A., and H.-G. Sockel, (2004) *Mater. Sci. Eng.*, A**366**, 87.
Rao, K.T. Venkateshwara, S.C. Siu, and R.O. Ritchie, (1993) *Metall. Trans.*, **24A**, 721-734.
Rezai-Aria, F., T. Liechti, and G. Gagnon, (1993) *Scripta Metall. Mater.*, **28**, 587-592.
Roebuck, B., E.A. Almond, and A.M. Cottenden, (1984) *Mater. Sci. Eng*, **66**, 179.
Salazar, A., J.Y. Pastor, and J. LLorca, (2004) *IEEE Trans. Appl. Supercon.*, **14**, 1941-1947.
Sanders, B.P., and S. Mall, (1996) *J. Comp. Tech. Res.*, **18**, 15-21.
Seeger, A., J. Diehl, S. Mader, and H. Rebstock, (1958) *Phil. Mag.*, **2**, 323.
Shang, J.K., W.K. Yu, and R.O. Ritchie, (1988) *Mater. Sci. Eng.* **A102,** 181–192.
Shen, Y.-L., M. Finot, A. Needleman and S. Suresh, (1995) *Acta Metall. Mater.*, **43**, 1701.
Starke, E.A., and G. Luetjering, (1979) in *Fatigue and Microstructure,* J.T. Stayley and E.A. Starke, eds., American Society for Metals, pp 205-243.

Stoloff, N.S., (1978) in *Advances in Composite Materials*, p. 247. Applied Sci. Pub., London.

Sugimura, Y., and S. Suresh, (1992) *Metall. Trans.*, **23A**, 2231-2242.

Suresh, S., (1998) *Fatigue of Materials*, 2nd Ed., Cambridge University Press, Cambridge,UK.

Taylor, L.G., and D.A. Ryder, (1976) *Composites*, **1**, 27.

Vasudevan, A.K., K. Sadananda, and N. Louat, (1994) *Mater. Sci. Eng.*, **A188**, 1-22.

Vasudevan, A.K., and K. Sadananda, (1995) *Metall. Mater. Trans.*, **26**, 1221-1234.

Vyletel, G.M., D.C. Van Aken, and J.E. Allison, (1991) *Scripta Metall. Mater.*, **25**, 2405-2410.

Walls, D.P., G. Bao, and F.W. Zok, (1993) *Acta Metall. Mater.*, **41**, 2061-2071.

Walls, D.P., and F.W. Zok, (1994) *Acta Metall. Mater.*, **42**, 2675-2681.

Wu, G., and J.-M. Yang, (2005) *JOM*, **57**, 72-79.

Xu, Z.R., K.K. Chawla, A. Wolfenden, A. Neuman, G.M. Liggett, and N. Chawla, (1995) *Mater. Sci. Eng.*, **A203**, 75.

Zhang, T., and H. Ghonem, (1995) *Fatigue. Fract. Eng. Mater. Struc.*, **18**, 1249-1262.

Zhang, W., M. Gu, J. Chen, Z. Wu, F. Zhang, H.E. Deve´, (2003) *Mater. Sci. Eng.*, **A341**, 9-17.